Fractal clusters

B. M. Smirnov

Institute of Thermal Physics, Siberian Branch of the Academy of Sciences of the USSR, Novosibirsk
Usp. Fiz. Nauk **149**, 177–219 (June 1986)

Fractal clusters, i.e., systems formed as a result of the aggregation of solid particles executing Brownian motion in space, are discussed. Studies of fractal clusters and of the dynamics of their formation, based on modern computational techniques, are reviewed. Experimental studies of fractal clusters, and processes and phenomena in which they manifest themselves, are examined. An analysis is given of a model of ball lightning in which the active material has the structure of a fractal cluster.

CONTENTS

1. INTRODUCTION

Fractal clusters, or fractal aggregates, are commonly taken to be structures formed as a result of the aggregation of solid aerosols in a gas, when their motion is diffusion-limited. A fractal cluster has the characteristic branched structure. Intensive studies of such structures by the methods of computational physics have been carried out in recent years. Numerical simulations have resulted in a reasonably complete picture of such structures and of the nature of their formation.

Fractal clusters formed as a result of the aggregation of solid particles, and the process leading to this, have connections and analogies with a number of other physical systems and processes. These include processes and structures involved in the formation of clusters, solidification of colloidal solutions, coagulation, percolation, formation of polymers, dielectric breakdown, certain biophysical processes, and so on. Although each of these problems has its own specific features, general ideas on fractal clusters provide us with a basis for a more fundamental analysis of systems and phenomena, and hence a higher level of sophistication in these studies.

Fractal clusters are directly related to processes of aggregation of solid particles, such as the formation of clusters in clouds, coagulation of particles in smoke, formation of structures during the relaxation of metallic vapor, and so on. Such processes may have a significant effect on a given resultant process or phenomenon. However, since they constitute an intermediate stage of the resultant process, they cannot readily be exposed because of difficulties in recording and analysis of such effects. An understanding of the physics of the formation of fractal structures changes the situation in relation to the study of such systems. Experience has shown that the major experimental studies of fractal structures have been based on theoretical ideas on such systems. Hence, an extension of these ideas should facilitate further experimental studies in this area and, consequently, the evolution of the true physical picture of these structures and processes.

Fractal structures are also interesting in connection with the elucidation of the nature of ball lightning. Of all the existing models of this phenomenon, the only one capable of explaining the spherical shape and constant size of ball lightning in the course of its evolution is that in which the active material has the structure of a fractal cluster. The consequences ensuing from the fractal structure of the active material of ball lightning enable us to analyze certain properties of the phenomenon and to mark out further possible lines of research.

Our aim has been to review theoretical studies of fractal clusters and the dynamics of their formation, to analyze experimental data on the evolution of such structures, and to examine real systems in which such structures appear.

2. FRACTAL STRUCTURES

Let us imagine how one might construct a fractal structure consisting of individual particles in the simplest formulation of the problem. We shall confine our attention to the two-dimensional case, and construct the cluster in accordance with the Witten-Sander model.[1] Accordingly, we shall divide bounded two-dimensional space into a set of square cells. We shall then insert one particle into this space and continue adding one particle at a time. Each new particle will move to a neighboring cell in a random manner, its path being chosen by the Monte Carlo method. When a particle reaches the boundary of our space, it is reflected. The motion of the particle continues until it is found to be in the neighborhood of one of the particles in the cluster. It is then brought to rest and fixed in the particular cell, and the next

 0038-5670/86/060481-25$01.80 © 1987 American Institute of Physics

particle is allowed to enter the space. This method can be used to "grow" a fractal cluster.[1)] The Witten-Sander model has played an important part in the study of fractal clusters because it provided a simple way of producing such clusters. It was the point of departure for extensive investigations of these structures which, in a relatively short time, led to a clear physical picture of these systems.

A fractal cluster exhibits the general properties of fractal systems.[2–4] The parameters that conveniently describe such systems will be introduced later, and our main interest in this review will be in geometric fractal systems. Let us take the coastline as a simple illustration of a fractal system that is close to the objects that we shall investigate.[2] Let us suppose that we measure the length of the coastline between two points. Since the coastline is irregular, the result we shall obtain will depend on the basic scale of the measurement that we shall adopt. For example, as a first step, we might distribute beacons along the edge of the land, so that the separation between neighboring beacons is 1 km. The length of the coastline in kilometers can then be taken to be the number of such beacons. We next perform a similar measurement except that, this time, the separation between the beacons is reduced by a factor of 10. In the third measurement, we follow the coastline on foot, without departing from the coastline by more than, say, 1 m. We take the length of the path traversed in this way as the length of the coastline. Finally, in the last case, we check our measurement by allowing an ant to crawl along the line without departing from it by more than the width of its body. Again, the length of the trajectory traversed by the ant is taken as the length of the coastline. It is clear that each of these measurements will yield a different result because the smaller the scale, the more closely we will be able to follow the irregular shape of the coastline. The length L of the coastline obtained in each case can be written in the form

$$L = a\left(\frac{R}{a}\right)^D, \tag{2.1}$$

where a is the scale size and R is the straight-line separation between the points. The parameter D is called the fractal dimension.

One of the simplest ways of producing fractal structures is based on the so-called Koch figures. To do this, let us take a segment of a straight line and use a particular algorithm (Fig. 1) to transform it into a broken line consisting of segments of equal length. The next operation is to transform each of these segments in accordance with the same algorithm and thus reduce the scale. Each of the new segments is again transformed in the same way, and still smaller scale is obtained. This operation can be repeated many times and eventually leads to a corrugated line with a fine structure. Figure 2 shows an example of such a line after four transformations of a segment. In accordance with the chosen algorithm, each operation corresponds to a choice of scale that is smaller by a factor of 4, and to the appearance of eight segments after the transformation. After a fourfold transformation, the length of the broken line in Fig. 2 increases by the factor $2^4 = 16$ and the scale is reduced by the factor $4^4 = 256$.

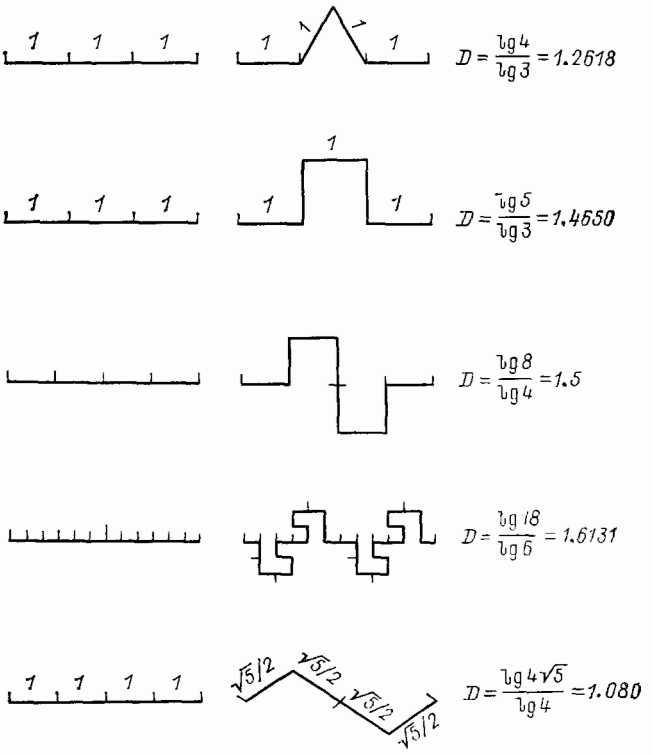

FIG. 1. Different variants of elements of Koch figures and their fractal dimensions.

Let us now take a wire, divide it into a large number of identical segments of length l, and number these segments. We then use the wire to construct a Koch figure of minimum scale a that exceeds the length of an individual segment. Next, we introduce the correlation function

$$C(r) = \frac{1}{N}\sum_i \rho(\mathbf{r}_i)\,\rho(\mathbf{r}_i + \mathbf{r}) = \frac{\langle \rho(\mathbf{r}' + \mathbf{r})\,\rho(\mathbf{r}')\rangle}{\langle \rho(\mathbf{r}')\rangle}, \tag{2.2}$$

where N is the number of segments, i is the segment number, and ρ is the density that is equal to unity at an occupied point and zero at a point not occupied by the wire. Subsequently, when we consider a cluster, the wire segments will be replaced with the particles of which the wire consists.

If we now modify slightly the regular structure of the Koch figure and average over the angles of the vector $\mathbf{r}$, the correlation function will correspond to the mean density of the wire at a distance r from occupied points. Since the mass of the wire in the sphere of radius r, centered on an occupied point ($r \gg a$), is proportional to r^D, the mean density at this distance is proportional to r^{D-d}, where d is the dimension of the space into which the wire is inserted. The correlation function thus becomes

$$C(r) = \frac{\text{const}}{r^{\alpha}}, \tag{2.3}$$

where r is much greater than the length of a minimum structure of the line, and

$$D_\alpha = d - \alpha. \tag{2.4}$$

We now turn to the fractal cluster under investigation. It consists of a set of particles "glued" together, whose size

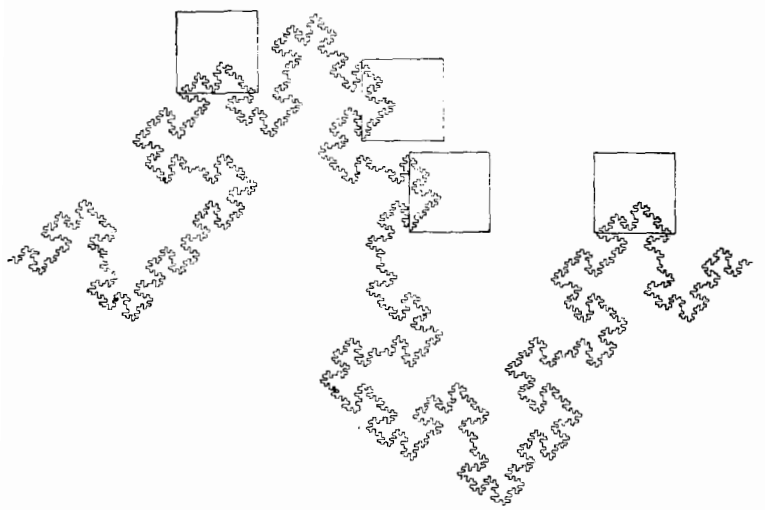

FIG. 2. Koch figure obtained from a segment after four transformations in accordance with the algorithm given by the third example in Fig. 1. The squares contain identical pieces of the cluster.

(or the size of the cells occupied by them) is much smaller than the size of the cluster. This type of cluster is a set of connected, branched lines, whose minimum structural scale is of the order of the particle size a (Fig. 3). Hence, in a region of size

$$R \gg r \gg a, \tag{2.5}$$

where R is the size of a cluster, the cluster correlation function (2.2) will satisfy (2.3). Figure 4 shows the correlation function for a fractal cluster assembled in accordance with the Witten-Sander model.[1] This figure confirms that the fractal cluster is, in fact, a fractal structure.

However, as a geometric system, a fractal cluster has a simpler physical significance because it exists in coordinate space. One of the consequences of the method used to construct it is that the mean density of particles in the cluster decreases with distance from the center in accordance with (2.3), i.e., the density is of the form

$$\rho(r) = \frac{\text{const}}{r^{\alpha}}, \tag{2.6}$$

where r is the distance from the center. We can use this to find the relation between the cluster size R [2)] and the number N of particles it contains:

$$N \sim R^{D_\beta}, \quad R \sim N^{\beta}, \quad \beta = \frac{1}{D_\beta}, \tag{2.7}$$

where the fractal dimension D_β must be the same as the quantity D_α in (2.4).

Fractal systems have the property of self-similarity. In particular, if, in the neighborhood of a point occupied by a cluster, we consider a region of relatively small volume, the portions of the cluster that will fall into it will be similar in the physical sense of this word. In particular, for a regular cluster, this law can be used to select identical segments. To confirm this, Fig. 2 shows a number of regions (squares) containing identical pieces of the cluster. In the case of a cluster with a random disposition of particles, self-similarity must be understood in the statistical sense, i.e., if we cut a large number of pieces found in equal volumes at different

FIG. 3. Typical fractal cluster obtained in a computer experiment simulating the aggregation of solid particles in the Witten-Sander model.[1]

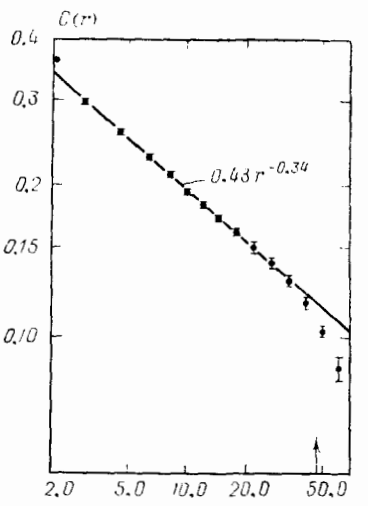

FIG. 4. Correlation function (2.2) averaged over six clusters obtained in the Witten-Sander model.[1] The results are given in units of the lattice constant, and the arrow shows the position of the average radius of gyration. The indicated uncertainties are the average statistical uncertainties for six clusters.

points in the cluster, we find that, on average, they will contain the same number of particles. This conclusion follows directly from (2.2) and (2.3) if we apply them to individual portions of the cluster.

We note that the self-similarity of a fractal cluster is in apparent contradiction with the conclusion drawn from (2.3) that, as the cluster size increases, the mean particle density in the cluster decreases in accordance with (2.6). However, this contradiction is removed by more careful analysis. Actually, an increase in the size of a cluster is accompanied by an increase in the volume of empty spaces, and large empty spaces, which do not affect the mean density of particles in a small occupied volume of the cluster, provide a significant contribution to its overall mean density.

The important point is that a fractal cluster constructed according to a random law, and therefore appearing to be an unordered system, nevertheless has internal order. The parameter characterizing this order is the fractal dimension of the cluster. Proper understanding of this fact enables experimenters to perform more detailed studies of such systems, and experience gained in the last few years has confirmed this.

It follows from the above formulas that the fractal dimension of a cluster can be found in two ways, namely, from (2.3), using the correlation function, and from (2.7), using the number of particles in clusters of different size, or in individual portions of the cluster that have different sizes. Since (2.3) and (2.7) are valid on average, the result obtained by either method is subject to an uncertainty, and the two methods lead to somewhat different results. To demonstrate this, let us consider how we might determine the fractal dimension of the cluster shown in Fig. 5. In accordance with (2.1), the fractal dimension of this cluster is $D = \log 10/\log 4 = 1.66$ (we have specially chosen a cluster whose fractal dimension is close to the corresponding cluster parameter obtained in the Witten-Sander model). Clearly, if the algorithm of Fig. 5a is repeatedly applied to a selected segment, and then a large number of portions of the cluster occupying different areas in space are examined, we find that (2.7) yields a value for the dimension that is close to the required value. In this case, the cluster is obtained after three transformations of a straight segment in accordance with the algorithm of Fig. 5a. Next, we compare the length of the portion lying inside rectangles with one side parallel to the initial segment and length equal to the length of this segment. Figure 6 shows the results of an analysis based on (2.7). Statistical examination of these data shows that the fractal dimension is $D_\beta = 1.64$ and the statistical uncertainty is 6×10^{-4}. Clearly, this result differs from the accurate value of the fractal dimension by just over 1%. The same scale of uncertainty is encountered in the analysis of model clusters (Tables I and II).

The Witten-Sander model has played an important part in the investigation of fractal clusters and is itself a way of simulating the assembly of a fractal cluster. The model can be modified. For example, we can abandon the subdivision of space into cells, and consider each particle in the form of a disk in two-dimensional space, or a sphere in three-dimensional space, and specify the trajectory of its motion in the form of the appropriate broken line. A collision of the particle with one of the particles in the cluster results in their coalescence. The particle is then fixed on the cluster in this position, and the next particle is let into the space. This model is referred to as a nonlattice model,[5] whereas the Witten-Sander model is a lattice model. Calculations show that, in the cases that have been examined, the results obtained from the two models agree to within their uncertainties. The next step is to introduce a probability P that, when two particles touch, they coalesce. This probability was previously assumed to be equal to unity.

The Witten-Sander model and its different modifications correspond to particular physical conditions for the formation of a fractal cluster: the cluster is assembled by adding individual particles to it. It is, however, possible to imagine a different physical situation in which a fractal cluster will be formed. A definite number of particles is intro-

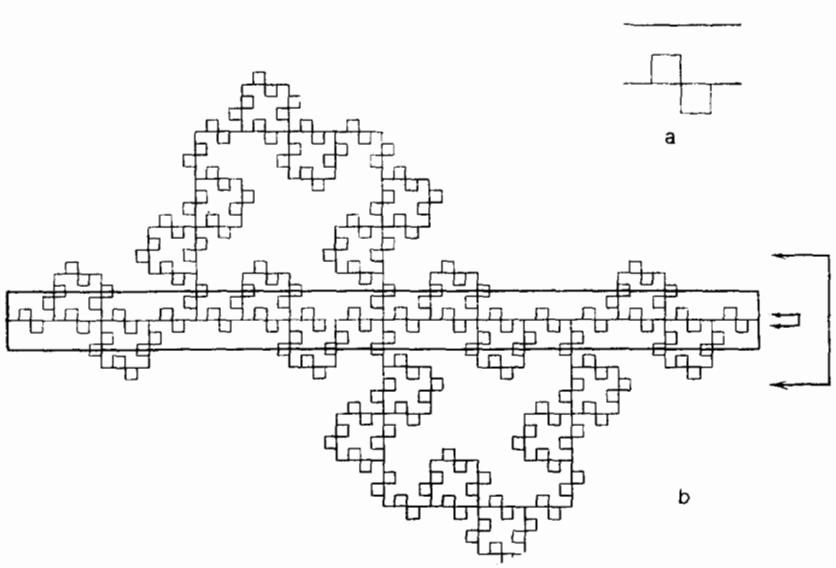

FIG. 5. Koch figure with fractal dimension $D = 1.66$ close to the fractal dimension of a two-dimensional cluster in the Witten-Sander model: a—algorithm used to transform a segment, b—cluster obtained after three transformations in accordance with this algorithm. Arrows show the size of rectangles containing pieces of cluster used to determine the fractal dimension from (2.7). One of these rectangles is shown in the figure.

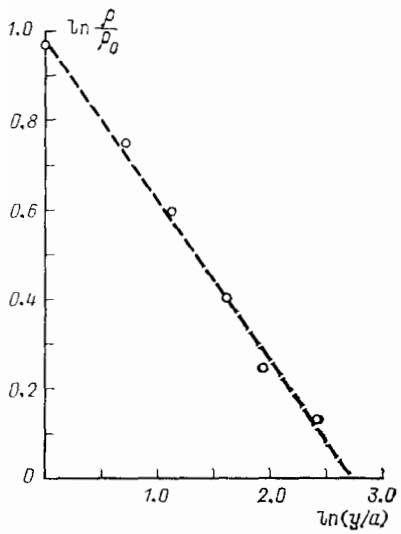

FIG. 6. Density of the cluster portion shown in Fig. 5, falling into the rectangle, as a function of the width of the rectangle. The density ρ is the ratio of the total length of the piece of cluster in the rectangle to the area of the rectangle, and is given in arbitrary units; the width y of the rectangle is given in units of the minimum scale. The broken line corresponds to a fractal dimension of the cluster equal to 1.64.

duced into the volume at an initial instant of time, and the particles coalesce when they collide with one another. This will initially result in the appearance of a large number of small clusters, and subsequent collisions will lead to their aggregation. Eventually, the number of clusters in the volume will fall, and the cluster size will rise. The fractal clusters produced in this way will be looser in comparison with the cluster produced in the Witten-Sander model because, in this method, it is more difficult to fill empty spaces.[3)]

So far, we have considered that the aggregating particles execute diffusion-limited motion in space, so that the particle mean free path is small in comparison with typical dimensions in the cluster. A different situation is physically possible in which the particle mean free path is large in comparison with the size of the region of coalescence. It can then be considered that the particle (or cluster) travels along straight lines. The results obtained by studying fractal clusters produced by the above methods are summarized in Tables I and II. These data were obtained by analyzing calculations based on the corresponding models. The quoted uncertainties are statistical, and were obtained by analyzing formed clusters. It is clear that, as in Fig. 5, this uncertainty amounts to a few percent. Table III lists the average values of the fractal dimension obtained from the data of Tables I and II, and corresponds to the coalescence probability $P = 1$. The uncertainty shown in Table III is a measure of the agreement between the different results listed in Tables I and II.

As geometric systems, fractal clusters formed by the aggregation of solid particles should appear when aerosols aggregate in a gas (they can also appear during the relaxation of a metallic vapor and its deposition on a surface, during the formation of clouds and mist, and during the coagulation of aerosols in smoke), and also when clusters are formed from particles in suspensions and colloidal solutions. The structures that we are considering have a direct significance in relation to these problems. However, this does not exhaust the range of problems in which ideas on fractal structures may be useful. Figures 7 and 8 illustrate structures that have analogies with fractal clusters.

In accordance with the traditional introduction of the

TABLE I. Fractal dimension of a cluster produced by aggregation of solid particles in two-dimensional space.

Aggregation model	Attachment probability P	Fractal dimension of cluster	
		D_α	D_β
1. Rectilinear trajectory, particle-cluster	$P=1$	1.92±0.1 [8,16]	1.95±0.02 [8,16] 1.99±0.01 [10] 2.00±0.02 [11]
2. Brownian motion, particle-cluster	$P=1$	1.657±0.004 [1] 1.68±0.07 [5] 1.68±0.05 [12]	1.70±0.02 [1] 1.68±0.04 [5] 1.69±0.05 [12] 1.71±0.04 [11] 1.660±0.004 [14]
	$P=0.25$	1.71±0.05 [5] 1.74±0.03 [5] 1.70±0.03 [5]	1.73±0.04 [5] 1.73±0.05 [12] 1.73±0.06 [13]
	$P=0.1$	1.73±0.03 [12]	1.71±0.06 [12] 1.78±0.06 [13] 1.69±0.06 [13]
	Capture at four particle diameters		
3. Rectilinear trajectory, cluster-cluster	$P=1$	1.55±0.02 [15] 1.54±0.03 [15]	1.50±0.05 [15] 1.56±0.02 [15]
4. Brownian motion, cluster-cluster	$P=1$	1.48±0.03 [6] 1.39±0.05 [7] 1.48±0.02 [15] 1.46±0.02 [18*)] 1.479±0.017 [19*)]	1.45±0.05 [6] 1.37±0.08 [7] 1.42±0.03 [9,21] 1.44±0.02 [15] 1.44±0.01 [18*)] 1.442±0.014 [19*)]
	$P=0.1$	1.45±0.04 [18]	1.46±0.03 [18]

*)Average over different models

TABLE II. Fractal dimension of a cluster produced by aggregation of solid particles in three-dimensional space.

Aggregation model	Attachment probability P	Fractal dimension of cluster	
		D_α	D_β
1. Rectilinear trajectory, particle-cluster	$P=1$		2.97 ± 0.03 [8]
2. Brownian motion, particle-cluster	$P=1$	2.49 ± 0.06 [12] 2.45 ± 0.2 [18,22] 2.39 ± 0.2 [22] 2.39 ± 0.19 [23]	3.0 [11] 2.51 ± 0.06 [12] 2.54 ± 0.02 [11] 2.45 ± 0.10 [22] 2.49 ± 0.19 [23]
	$P=0.25$		2.48 ± 0.12 [12]
3. Rectilinear trajectory, cluster-cluster	$P=1$	1.95 ± 0.05 [15] 1.98 ± 0.04 [15]	1.81 ± 0.03 [15] 2.00 ± 0.05 [15]
4. Brownian motion, cluster-cluster	$P=1$	1.8 ± 0.1 [15] 1.76 ± 0.08 [55] 1.83 ± 0.05 [55]	1.75 ± 0.05 [15] 1.72 ± 0.10 [17] 1.78 ± 0.05 [20,21] 1.76 ± 0.05 [55]

fractal dimension of a cluster on the basis of (2.3) and (2.4), a fractal cluster has an analogy with other fractal structures formed in different processes.[27] For example, in the case of turbulence, the correlation function analogous to (2.2) is

$$\langle \varepsilon(\mathbf{r}')\,\varepsilon(\mathbf{r}'+\mathbf{r})\rangle = \bar{\varepsilon}^2\left(\frac{l_0}{r}\right)^{d-D}, \tag{2.8}$$

where ε is the mean energy per unit mass of the liquid or gas processed per unit time, and $l_d \ll r \ll l_0$, where l_d is the typical length for energy dissipation and l_0 is the typical mixing length. Analysis shows[28,29] that the fractal dimension corresponding to turbulence in three-dimensional space ($d=3$) is $D=2.5$–2.75.

3. PROPERTIES OF FRACTAL CLUSTERS

Studies of fractal clusters performed in recent years by the methods of computational physics are the basis for our ideas about these objects. These studies have also demonstrated the possibilities of modern computational physics. On the one hand, by varying the individual parameters, we can use these models to provide a good approximation to the formation of fractal structures. On the other hand, they give us a ready-made object, with all its properties, which enables us to perform a comprehensive analysis of the object and, through comparison, identify those of its properties that are universal. Computer simulations of the evolution of fractal clusters are thus the source of our current ideas on such objects. We now turn to a presentation of our knowledge of fractal clusters, obtained by analyzing the results produced by computer simulations.

To investigate the structure of a fractal cluster, let us follow its evolution within the framework of the Witten-Sander model. Particles moving away from the cluster periphery and toward its center encounter its core and become attached to it. The diffusion-limited motion of a particle facilitates its penetration of the cluster over a wide area, and this increases the probability that the particle will bind to the cluster at a peripheral point. This process is conveniently examined by introducing the cluster penetration depth for a new particle. Let us consider this problem in the language of the particle penetration depth.

Let $P(r, R)$ be the probability that a given test particle attaches itself to a cluster of size R at a distance r from the center. If the cluster penetration depth of the particle, Δr, is much less than the size of the cluster, the probability is conveniently approximated by the expression[10]

$$P(r,\ R) = \frac{1}{(2\pi)^{1/2}\,\Delta r}\exp\left[-\frac{(R-r)^2}{2\Delta r^2}\right], \tag{3.1}$$

where we use the normalization condition

$$\int_0^R P(r,\ R)\,\mathrm{d}r = 1.$$

We have taken the simplest expression for the required func-

TABLE III. Fractal dimension of a cluster formed by aggregation of solid particles.

Aggregation model	Dimension of space	
	2	3
1. Rectilinear trajectory, particle-cluster	2	3
2. Brownian motion, particle-cluster	1.68 ± 0.02	2.46 ± 0.05
3. Rectilinear trajectory, cluster-cluster	1.54 ± 0.03	1.94 ± 0.08
4. Brownian motion, cluster-cluster	1.44 ± 0.04	1.77 ± 0.03

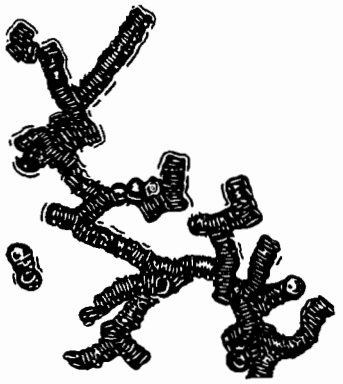

FIG. 7. A column of erythrocytes formed in a suspension of blood by the aggregation of red cells.[25]

tion that satisfies the physical conditions of the problem.

The formula given by (3.1) gives us a perfectly specific expression for the mean density of particles in a cluster near its edge. In particular, since the depth of penetration is small in comparison with the cluster size, we find from (3.1) that the mean particle density in the cluster near its edge is

$$\rho = \rho(r_0)\,\Phi\left(\frac{R-r}{\sqrt{2}\,\Delta r}\right), \tag{3.2}$$

where $\rho(r_0)$ is the mean density of particles near the cluster edge at points where the evolution of the cluster is complete, i.e., for $R \gg R - r_0 \gg \Delta r$, and $\Phi(x)$ is the probability integral, such that $\Phi(x \ll 1) = 2x/\pi^{1/2}$ and $\Phi(\infty) = 1$.

Combining (2.6) and (3.2), we find that the mean density of particles in the cluster is

$$\rho(r) = \rho_0\left(\frac{r_0}{r}\right)^{\alpha}\Phi\left(\frac{R-r}{\sqrt{2}\,\Delta r}\right). \tag{3.3}$$

Hence, recalling that $\Delta r \ll R$, we find that the total number of particles in the cluster is

$$N = \int_0^R 4\pi r^2\,dr\cdot\rho(r) = 4\pi\rho_0 r_0^{\alpha}\frac{R^D}{D}\left[1-\left(\frac{2}{\pi}\right)^{1/2}D\,\frac{\Delta r}{R}\right], \tag{3.4}$$

where $D = d - \alpha$ is the fractal dimension of the cluster and the expression for the density of states refers to the three-dimensional case ($d = 3$) although, apart from a numerical factor, the resulting expression is suitable for clusters in spaces of arbitrary dimension.

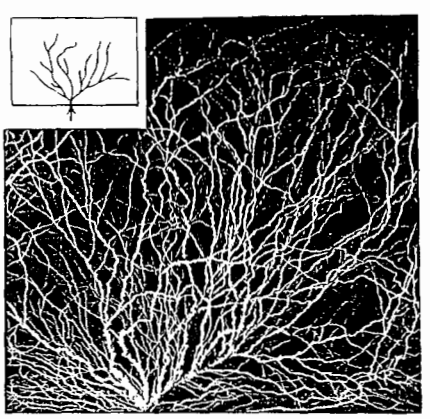

FIG. 8. Structure of electric breakdown on the surface of a dielectric.[26]

We shall now use the above formulas to compare the values of the fractal dimension obtained by two different methods. The first involves the analysis of (2.2) for distances small in comparison with the cluster size but large in comparison with the size of an individual particle. The correlation function is now constructed for this cluster and, according to (2.3) and (2.4), enables us to find its fractal dimension. This operation is shown in Fig. 3. In the other method, the fractal dimension is determined from (3.4), which yields

$$\frac{dN}{N} = D\left[1+\left(\frac{2}{\pi}\right)^{1/2}\frac{\Delta r}{R}\right]\frac{dR}{R}. \tag{3.5}$$

The fractal dimension of the cluster can be obtained from this result in the limit as $\Delta r/R \to 0$. Actually, the resulting value is somewhat too high:

$$D_\beta = D\left[1+\left(\frac{2}{\pi}\right)^{1/2}\frac{\Delta r}{R}\right]. \tag{3.6}$$

We must now estimate the particle penetration depth Δr as a function of the parameters of the problem. Since the particle undergoes Brownian motion, we have $\Delta r^2 \sim \mathscr{D}\tau$, where $\mathscr{D}$ is the particle diffusion coefficient and τ its lifetime inside the cluster. Moreover, $\mathscr{D} \sim v\lambda$, where v is the characteristic velocity of the particle and λ is its mean free path, i.e., the length over which it changes its direction of motion. In this particular case, the mean free path is of the order of the size of an individual cell. Moreover, $1/\tau \sim \rho v\sigma$, where ρ is the mean particle density and the attachment cross section σ does not depend on R. Since, in the main part of the cluster, $\rho \sim R^d/n$, where d is the dimension of the space, we obtain

$$\Delta r \sim R^{(d-D)/2} \sim N^{(d-D)/2D}. \tag{3.7}$$

We now introduce the parameter ν through the relation

$$\Delta r \sim N^{\nu}, \tag{3.8}$$

and then use (3.7) in the two-dimensional and three-dimensional cases (see Tables I and II) to show that $\nu \simeq 0.1$. This result is in conflict with the direct analysis of cluster growth within the framework of the Witten-Sander model, which gives $\nu = 0.48 \pm 0.01$ in the two-dimensional case[10] and $\nu = 0.32 \pm 0.05$ in the three-dimensional case.[30] The reason for this discrepancy is that we assumed in the calculation of the test-particle attachment probability that the cluster particles were distributed randomly in space. This assumption is clearly invalid. The branched structure of the cluster enables the aggregating particles to penetrate the cluster much more deeply than in the case of a random distribution of cluster particles in space with the same mean density.

It follows from the above calculations that, as the fractal cluster size increases, the particle penetration depth increases more slowly than its size. In fact, in the above calculations, the ratio of the penetration depth index ν and the cluster size index D_β is $p = \nu D_\beta = 0.82 \pm 0.04$ in the two-dimensional case and $p = 0.80 \pm 0.14$ in the three-dimensional case. It is concluded in Ref. 30 that this ratio tends to unity for a large cluster. An increase in the number of particles in the cluster by an order of magnitude (up to 50 000

particles in the cluster) leads to the result $p = 0.93 \pm 0.01$ in the two-dimensional case.[30]

Interesting information about fractal clusters is provided[12] by the mean coordination number, i.e., the average number of nearest neighbors of a cluster particle. This mean coordination number has been found for the case where the cluster is formed by attachment of one particle at a time, the motion of each particle being diffusion-limited in space. For unit particle-attachment probability, the mean coordination number is 2.202 ± 0.017 for the two-dimensional case and 2.251 ± 0.006 for the three-dimensional case. When the attachment probability is $P = 0.25$ in three-dimensional space, the mean coordination number is 2.514 ± 0.018. This quantity is not very sensitive to the details of the model. In the case of unit attachment probability in two-dimensional space, the mean coordination number is 2.191 ± 0.007 for a lattice model and 2.216 ± 0.019 for a nonlattice model. These values show that the successive branching occurs in these clusters on average in steps of 4–5 particles.

The fractal structure of the projection of a three-dimensional cluster on a plane was investigated in Ref. 12. This analysis is of practical value because the structure of a three-dimensional cluster is actually deduced from a photograph recorded in an electron microscope, i.e., from a projection of the cluster on a plane. When the three-dimensional cluster is formed in the above case by the successive attachment of individual particles executing Brownian motion in space, the projected area S of the cluster is related to the number N of particles in the cluster by

$$S \sim N^{\gamma}. \tag{3.9}$$

If the three-dimensional cluster were optically transparent, i.e., the projections of individual particles were to fall on different points, we would have $S \sim N$, i.e., $\gamma = 1$. This occurs for clusters with a low particle density.

However, a cluster containing a large number of particles is optically opaque at the center and, as the number of particles increases, the size of the opaque region near the center is also found to increase. Hence, $\gamma < 1$. For a compact cluster, we then have $\gamma = 2/3$, i.e.,

$$\frac{2}{3} < \gamma < 1. \tag{3.10}$$

It has been found[12] that, for a cluster obtained by diffusion-limited particle-cluster aggregation, with particle-attachment probability on contact equal to unity, the required parameter is $\gamma = 0.864 \pm 0.003$. When $P = 0.25$, the cluster becomes more compact and the parameter γ is accordingly reduced: $\gamma = 0.830 \pm 0.016$.

We shall now use these results to analyze the above cluster from another point of view, in which it is regarded as a radiating body. In this case, its effective surface area S_{eff} responsible for the emission is greater by a factor of four than the mean projected area, i.e., $S_{\text{eff}} = 4S$. Let us compare this with the surface area S_0 of a sphere into which the cluster can be inserted. First, we consider the physical limiting cases. When the system is dense enough, i.e., we consider only those particles that lie on the surface, we have $S_{\text{eff}} = 4S_0$. We now introduce the relation

$$\frac{S_{\text{eff}}}{S_0} \sim N^k, \tag{3.11}$$

where N is the number of particles in a cluster, and we find that $k = 0$ for an optically thick cluster. For an optically transparent system, in which each particle can be "seen," i.e., none of the particles is obscured by other particles, we have $S_{\text{eff}} \sim N$, $S_0 \sim N^{2/3}$, or $k = 1/3$. All real cases must lie between these two limits:

$$0 < k < \frac{1}{3}. \tag{3.12}$$

We now turn to a real cluster. Since $S_{\text{eff}} \sim N^{\gamma}$ and $S_0 \sim R^2 \sim N^{2/D_\beta}$, we have

$$k = \gamma - \frac{2}{D_\beta}. \tag{3.13}$$

Bearing in mind the above values of γ (Ref. 12), and using the fractal dimension of the three-dimensional cluster (see Table II), we find that, for a fractal cluster obtained with unit particle-cluster attachment probability on contact ($D = 2.47 \pm 0.03$), the above index is $k = 0.054 \pm 0.013$. For a three-dimensional cluster formed by the attachment to it of individual particles executing Brownian motion in space with attachment probability of 0.25 ($D = 2.48 \pm 0.12$), we have $k = 0.024 \pm 0.045$. The fractal cluster is optically thick near the center and optically transparent on the periphery. These results indicate that the systems we have investigated are closer to optically dense objects.

The above results refer to a cluster assembled by the attachment to it of one particle at a time. The fractal cluster formed from smaller clusters, which, in turn, were formed by the attachment of finer clusters, is looser. It is, in fact, transparent and its projected area can be analyzed in a simpler way. In this approach we assume that the cluster consists of cylindrical fibers, and its branched structure gives rise to the corresponding fractal dimension. Suppose that the radius of an individual fiber is a and the average fiber length is much greater than the radius, so that the regions in which fibers join can be neglected. Since the fibers are distributed in space at random angles, we can average over these angles and find that a fiber of length l gives an average projected area on a plane equal to $(\pi/2)la$.

The probability that light will pass through a cluster along a given line is $1 - e^{-u}$, where u is the optical thickness of the cluster in the given direction. Whenever the optical thickness of the cluster is small, shadows due to individual fibers will not overlap, and the projected area of this part of the cluster on the plane will be equal to the sum of the projected areas of the individual fibers. The optical thickness of a cluster in a given direction z is $u = \int \mathrm{d}z/\lambda$, where $\lambda = \mathrm{d}V/\mathrm{d}S = \mathrm{d}V/(\pi/2)a\mathrm{d}L$ is the photon mean free path for the given point in the cluster, so that $\mathrm{d}L$ is the total length of fibers in an elementary volume $\mathrm{d}V$. We now introduce the mass density of the fiber material in the condensed state, ρ_c, and the mean mass density ρ of aerosols in the given region such that the mass of fibers in a given cluster element is

$$\mathrm{d}M = \rho_{\text{H}}\pi a^2\,\mathrm{d}L = \rho\,\mathrm{d}V.$$

Hence, since the mean cluster density at a distance r from its

center of mass is $\rho(r) \sim r^{-1.22}$ [in accordance with (2.3) and the data of Table III], we have

$$u = \int_{-\infty}^{+\infty} \frac{\pi}{2} a \frac{dL}{dV} dz = \int_{-\infty}^{+\infty} \frac{\rho(r)\, dz}{2a\rho_c}$$

$$= \frac{b\rho(b)}{2a\rho_c} B(0.11;\ 0.5) = 5.2 \frac{b\rho(b)}{a\rho_c}, \qquad (3.14)$$

where b is the minimum distance between the cluster center and the ray, and $b \ll R$, where R is the cluster size.

It follows from the above formula that the optical thickness of a cluster is of the order of unity only when the ray passes through the cluster near its center ($b \sim a$). The optical thickness of the main part of the cluster is small, i.e., the projected cluster area on the chosen plane is equal to the sum of the projected areas of the individual cluster elements on this plane.[4)]

The particular feature of the fractal cluster formed in the Witten-Sander model is that, when it is small, it is anisotropic.[24,31] Indeed, during the early stage of its assembly, new particles are attached with high probability to the ends of the cluster, which tends to emphasize its anisotropy. However, as the cluster size increases, so that the particle penetration depth becomes smaller than its overall size, the cluster grows uniformly in all directions. The cluster anisotropy therefore diminishes as it grows.[5)]

The nonspherical shape of the cluster assembled in the Witten-Sander model was investigated in detail in Ref. 24. The principal axes x, y, z of the cluster were determined by diagonalizing the density tensor. The anisotropy is most clearly defined for a cluster formed in two-dimensional space. The ratio of the cluster lengths in the direction of the principal axes of the two-dimensional cluster containing 200 particles is $R_x/R_y = 0.69 \pm 0.13$, whereas for a cluster consisting of 50 000 particles, this ratio is 0.87 ± 0.07. The corresponding fractal dimensions of a cluster consisting of 2000 particles are $D_x = 1.61 \pm 0.05$, $D_y = 1.80 \pm 0.06$, and for a cluster consisting of 50 000 particles $D_x = 1.69 \pm 0.03$, $D_y = 1.75 \pm 0.03$. As can be seen, the departure from spherical symmetry decreases with increasing cluster size. The nonspherical shape of the three-dimensional fractal cluster is much less noticeable. Thus, for a Witten-Sander cluster of 12 500 particles, $D_x = 2.36 \pm 0.19$, $D_y = 2.54 \pm 0.19$, $D_z = 2.58 \pm 0.20$ (Ref. 24). As can be seen, the fractal dimensions of this cluster are the same to within the quoted uncertainties. It is important to note that the cluster becomes essentially anisotropic[32] for an anisotropic interaction potential between neighboring particles in the cluster and, consequently, for an anisotropic law of attachment of particles in the course of cluster assembly and in the limit of a large number of particles in the cluster.

The above fractal cluster has a loose structure, and is formed when the motion of a particle attaching itself to the cluster is diffusion-limited in space. On the other hand, if the particle attaching itself to the cluster moves rectilinearly in space, a compact cluster is formed in the two-dimensional space, so that its fractal dimension is practically the same as the fractal dimension of the space in which it is moving. The structure of a fractal cluster formed as a result of the successive attachment of particles to the cluster is thus determined by the fractal parameters of the trajectory followed by the particles in space. Hence, it is interesting to examine how the properties of a fractal cluster depend on the fractal properties of the trajectory of a particle attaching itself to the cluster.

This was considered by Meakin,[33] who examined the trajectories of particles consisting of rectilinear segments such that the probability $P(x)$ that the length of a successive segment was x was given by

$$P(x < 1) = 0,$$
$$P(x \geqslant l) = l^{-f}. \qquad (3.15)$$

The case $f = 0$ corresponds to motion over rectilinear trajectories, and $f = \infty$ corresponds to the Witten-Sander model. Table IV lists the fractal dimensions of a cluster for intermediate values of f. The results obtained for lattice and nonlattice models are similar, and the uncertainty quoted in Table IV is a measure of this agreement. Moreover, we note the connection between the parameter f and the fractal dimension of the particle trajectory. For $1 < f < 2$, the fractal dimension D of a particle trajectory is equal to the value of f ($D = f$). When $f \leqslant 1$, we have $D = 1$, and for $f \geqslant 2$ the result is $D = 2$. It follows from Table IV that, as the fractal dimension of the trajectory of the particle that subsequently attaches itself to the cluster increases, the resulting cluster becomes looser.

The previously studied fractal clusters were grown by the attachment of individual particles. In practice, a thread, wire, or substrate can act as the base for the aggregation of solid particles. The resulting cluster then has a somewhat different structure as compared with the situation where it is grown from individual particles. Such clusters were studied in Ref. 34. In accordance with the general property of fractal clusters, they become increasingly looser as the cluster size increases. The generation radius R_g of a cluster growing on a thread or fiber is related to the number N of particles in the cluster by $R_g \sim N^{\delta}$, where $\delta = 0.665 \pm 0.031$ ($D_\beta = 1.50 \pm 0.07$).

When the cluster grows on a thread, the length of the latter is much greater than the transverse size of the cluster, i.e., the initial conditions have an important influence on the evolution of the cluster. Similar conditions are chosen for a cluster evolving on a plane. In the two-dimensional case, the cluster grows on the plane on one side of a line whose length is much greater than the lateral size of the cluster. In the three-dimensional case, the cluster grows up from a plane, and the linear size of the plane on which the cluster evolves is

TABLE IV.

f	D_α	D_β
4/3	1.87±0.01	1.86±0.02
5/3	1.80±0.01	1.85
2	1.75	1.78±0.04
2.5	1.72±0.02	1.73±0.03

much greater than its height. All these examples can serve as models for real cases.

The parameter T describing a cluster growing on a plane is the square root of the mean square height of the cluster. The fractal properties of the cluster are determined by the dependence of this parameter on the number N of particles in the cluster: $T \sim N^{\varepsilon}$. For a compact cluster, $\varepsilon = 1$, and its fractal dimension $D_\beta = 1/\varepsilon$ is also equal to unity. For a loose cluster formed in the Witten-Sander model, the fractal dimension is lower. In the two-dimensional case, $\varepsilon = 1.300 \pm 0.075$ ($D_\beta = 0.77 \pm 0.04$), whereas in the three-dimensional case $\varepsilon = 1.7 \pm 0.2$ ($D_\beta = 0.59 \pm 0.07$). However, the power-type dependence of the cluster thickness on the number of particles in the cluster is valid for a massive cluster because, initially, the cluster has a very loose structure. Accordingly, the dependence of the cluster thickness on the number of particles within it is approximated by $T = 1.42 + 2.55 \times 10^{-4} N^{1.297}$ in the case of the two-dimensional cluster, and $T = 0.806 + 4.27 \times 10^{-6} N^{1.602}$ for a three-dimensional cluster. The unit of length is the length of cell that can be occupied by an individual particle.

Another characteristic feature of these clusters is the mean particle density $\rho(r)$, which decreases with increasing distance r from the thread or surface. This is described by (2.6), where, according to (2.4), $\alpha = d - D$ and d is the dimension of the space in which the cluster is formed (equal to two for a thread and unity for two-dimensional and three-dimensional clusters on a plane). If we use the correlation function (2.2) to find the fractional dimension of clusters, we find that for a cluster growing on a plane $D = 0.70 \pm 0.06$ in the two-dimensional case, whereas for a cluster growing on a thread $D = 0.050 \pm 0.06$ in the three-dimensional case. These data agree to within the stated uncertainties with the fractal dimensions D_β of these clusters, obtained from the dependence of their linear size on the number of particles within them. The above results[34] on fractal clusters formed on substrates of different shape can be used in the analysis of real systems.

The advances made in the study of the structure of fractal clusters have been made possible by modern computers which can be used to generate such objects in their memory, using appropriate algorithms. The required parameters of fractal clusters are obtained by direct analysis of the resulting objects, and the uncertainties of the calculated parameters are determined by the statistics of the results. Experience has shown that modern computers can be used to calculate the fractal dimension of clusters to within 1 or 2%. This means that the problem can be solved reliably in the computer, so that there is less interest in approximate analytic methods because the results obtained thereby are more problematic. We shall, nevertheless, review some of the analytic methods.

Hentschel[35] has examined the formation of a cluster by the successive attachment of individual particles, and has determined the fractal dimension of a cluster by minimizing its free energy. The expression for this energy was derived from simple considerations. The final expression for the fractal dimension of a cluster is[35]

$$D = \frac{4D_\omega + d(2D_\omega - 4) + 5d^2}{5D_\omega - 4 + 5d}, \tag{3.16}$$

where D_ω is the fractal dimension of the particle trajectory and d is the dimension of space. For Brownian motion ($D_\omega = 2$) in two-dimensional ($d = 2$) and three-dimensional ($d = 3$) spaces, this formula yields 1.75 and 2.52, which is not too different from the data listed in Tables I and II. However, it is clear that this formula is not accurate. In particular, it does not predict a compact cluster ($D = d$) for rectilinear trajectories ($D_\omega = 1$).

The fractal cluster formed in the Witten-Sander model was investigated in Ref. 36, where the mean-field approximation was developed. In this case, the theory involves the mean screening length, i.e., the cluster penetration depth of a particle, which is the same in all directions inside the cluster, but depends on the mean particle density in the cluster. This assumption leads to the following fractal dimension of the cluster:

$$D = \frac{d^2 + 1}{d + 1}. \tag{3.17}$$

In two-dimensional ($d = 2$) and three-dimensional ($d = 3$) spaces, this formula gives 1.67 and 2.5 for the fractal dimension, which agrees with the data of Tables I and II to within the stated uncertainties. However, for larger values of the dimension of space, there is a discrepancy between this formula and direct calculation.[5] Moreover, analysis shows[37] that the mean-field approximation is satisfactory only in three-dimensional space.

The hierarchical model[9] provides a simple way of constructing a cluster formed by the clustering of clusters. In this model, there are initially 2^k particles from which 2^{k-1} clusters are formed during the first stage. In the next stage, these clusters combine in pairs as a result of Brownian motion. Each successive stage leads to the pairing of clusters, so that the number of clusters is reduced by two and the number of particles in each of them increased by two. In the last stage, a single cluster consisting of 2^k particles is formed. Although the assembly of this cluster is simpler as compared with the general case, the fractal dimension of the cluster (1.42 ± 0.03; $d = 2$) is equal to the fractal dimension of the cluster formed in two-dimensional space by cl-cl aggregation (Table I).

The renormalization group approximation,[38–42] used in percolation problems, can also be extended to fractal clusters. In the case of a fractal cluster formed within the framework of the Witten-Sander model in two-dimensional space, the renormalization group approximation yields[42] $D = 1.67$–1.71, in agreement with the data in Table I.

When we consider the properties of a fractal cluster, we have in mind, above all, the physical problem of the aggregation of solid aerosols. Actually, these properties are manifested in many other physical phenomena, e.g., percolation, solidification of disperse systems (gel formation), polymerization, and so on, which all have their own specific problems, some of which may be fundamental. For example, in the percolation problem, one investigates the random walk of a particle over a cluster. The distance R traversed by the

particle in n steps (step length a) is given by the following expression for $n \gg 1$:

$$\frac{R}{a} \sim n^{\nu}. \tag{3.18}$$

In the case of diffusion-limited motion in free space, $\nu = 1/2$. The new fractal dimension $D_\omega = 1/\nu$ arises in this case. This is a fundamental parameter of the displacement of a particle in the region occupied (or unoccupied) by a cluster. Alexander and Orbach[43] conclude that the new fractal dimension is proportional to the fractal dimension of the cluster, so that

$$d_s = \frac{2D}{D_\omega} \tag{3.19}$$

is a universal quantity, independent of the dimension of the space. For a percolation cluster, the quantity d_s, called the spectral dimension, is equal to[43] 4/3. Subsequent investigations have shown that the spectral dimension depends on the type of the fractal cluster, i.e., on the model used to generate it.

The essential point is that the spectral dimension of a cluster can be related to the nature of the random walk of a particle over a cluster. We shall confine our attention to a lattice model and assume that the particle moves randomly from cell to cell. The probability of finding it at the initial point decreases with the time t[6] in accordance with the expression[43]

$$P_0(t) \sim t^{-d_s/2}. \tag{3.20a}$$

Next, the dependence on the mean number of different segments traversed by the particle is given by[44,45]

$$S_0(t) \sim t^{d_s/2}. \tag{3.20b}$$

Finally, the mean number of visits of the initial position is related to the time t since the beginning of motion by[46]

$$M_0(t) \sim t^{1-(d_s/2)}. \tag{3.20c}$$

Meakin and Stanley[47] have examined the Witten-Sander cluster and found the fractal dimensions describing the random walk of a particle on a cluster (see also Ref. 88). For two-dimensional space, they found that $d_s = 1.2 \pm 0.1$, $D_\omega = 2.56 \pm 1$, whereas for three-dimensional space $d_s = 1.3 \pm 0.1$, $D_\omega = 3.33 \pm 0.25$. More careful calculations performed in Ref. 14 have shown that, for two-dimensional space, $d_s = 1.205 \pm 0.018$, $D_\omega = 2.70 \pm 0.05$. It is clear that, although the Alexander-Orbach ratio ($d_s = 4/3$) does not hold for the fractal cluster obtained in the Witten-Sander model, the departure from this relation is not too serious.

Continuing our analysis of fractal parameters of a cluster, let us present one further way of finding the fractal dimension of a cluster, in addition to that based on (2.3) and (2.7). For simplicity, we consider the two-dimensional case and draw a contour around the cluster at a distance l from it. The rule used to construct this contour is as follows: any point on the contour must lie at a distance l from at least one point in the cluster, but none of the points in the cluster must lie at a distance less than l from any point on the contour. This contour has a less tortuous shape than the cluster itself and, as l increases, the contour "loses" all the new details of the cluster structure. When l is much smaller than the typical size of the cluster, the total length of the contour is given by[48,49]

$$S \sim l^{D-1}. \tag{3.21}$$

This relation was used in Ref. 14 to find the Witten-Sander fractal dimension of a cluster in two-dimensional space. The result was $D = 1.68 \pm 0.02$, and this is in agreement with the data in Tables I and III.

The convenience of using a computer to simulate the evolution of a fractal cluster lies in that different details of the process can be readily introduced into the model. This can be used to elucidate the sensitivity of the structure of the resulting system to different factors that are significant in real situations. The dependence of the fractal dimension of a cluster on the particle-attachment probability was discussed above (see Tables I and II). The lower the attachment probability, the greater the penetration of the cluster by the particle (in the Witten-Sander model), and the smaller the fractal dimension of the resulting cluster. However, calculations show (Tables I and II and Refs. 50 and 51) that this dependence is relatively weak. The other factor influencing the structure of the evolving cluster is rotational diffusion of the cluster. An increase in rotational diffusion leads to the trapping of particles or clusters by cluster edges, and facilitates a reduction in the fractal dimension of the resulting cluster. The effect of rotational diffusion on cluster structure in cluster-particle and cluster-cluster aggregation is investigated in Ref. 52.

In cluster-cluster aggregaton, the structure of the resulting cluster may depend on how the rate of cluster diffusion varies with cluster size. Calculations of cluster-cluster aggregation were carried out in Ref. 19 for different assumptions on the mass dependence of the diffusion coefficient. The fractal dimensions of clusters deduced for different laws expressing the dependence of the cluster diffusion coefficient on its mass are found to agree to within the reported uncertainties.

When specific processes are simulated, more specialized assumptions can be incorporated in the model. For example, we shall consider that, in cluster-cluster aggregation, the bond between the particles can rotate, or has a definite probability of breaking. Clusters must then come into contact at at least two points if stable bonds are to be formed. Calculations show[54] that, under these conditions, a more compact cluster is formed at short distances, and contains a large number of loops. However, at short distances, it has the same fractal dimension as in the absence of these effects.

Computer simulation of the evolution of fractal clusters can thus be used to elucidate the effect of different factors on their structure. The final result is a more or less complete picture of the possible structure in real situations.

4. DYNAMICS OF AEROSOL AGGREGATION

In addition to the structure of fractal aggregates, we have to investigate the dynamics of their evolution. Since such systems are formed as a result of the mutual attachment

of individual elements, useful information can be gleaned by studying the cluster size distribution at each instant of time, and the nature of its time dependence. It is clear that, in such problems, there are specific relationships between basic parameters, which do not change with time. In order to gain an understanding of the "scaling" that characterizes these problems, let us begin with the simplest problem of this kind, namely, the aggregation of liquid aerosols of relatively small size in a gas. Although this problem does not directly involve the objects that we have been investigating, it does enable us to gain an idea about the universality of the laws governing the process and the parameters that are convenient in its description.

In this problem, we have a set of liquid aerosols executing Brownian motion in a gas. When two aerosols collide, they coalesce into one. The latter is spherical in shape and takes part in the subsequent process. Our problem is to find the aerosol size distribution at an arbitrary time.

Let us first determine the rate of aggregation of aerosols of radius r_1 with the surrounding aerosols. We shall assume, to begin with, that a given aerosol is at rest, and all the others have radii r_2 and diffusion coefficients $\mathscr{D}_2$ in the gas. The density of these aerosols well away from the test aerosol is $N(\infty) = N_2$, and when these aerosols touch the test aerosol they are absorbed by it, i.e., $N(r_1 + r_2) = 0$. The diffusion flux of aerosols onto the test aerosol is $j = -\mathscr{D}_2(\mathrm{d}N/\mathrm{d}r)$, where r is the separation between the centers of the aerosols. Hence, it follows that the total flux of aerosols onto the test aerosol is

$$J = -4\pi r^2 \mathscr{D}_2 \frac{\mathrm{d}N}{\mathrm{d}r}. \tag{4.1}$$

Since there is no absorption of aerosols for $r > r_1 + r_2$, the flux J is independent of r. Solving (4.1) under the given boundary conditions, we finally obtain

$$J = 4\pi \mathscr{D}_2 (r_2 + r_1) N_2. \tag{4.2}$$

This is called the Smoluchowski formula.[57] Hence, we find that the aggregation rate constant for these aerosols is

$$k = \frac{J}{N_2} = 4\pi \mathscr{D}_2 (r_1 + r_2). \tag{4.3}$$

This expression was obtained on the assumption that the first aerosol was at rest. Clearly, when the diffusion-limited motion of the test aerosol is taken into account, we obtain the symmetric formula

$$k = 4\pi (\mathscr{D}_1 + \mathscr{D}_2)(r_1 + r_2), \tag{4.4}$$

where $\mathscr{D}_1$ is the diffusion coefficient of the test aerosol in the gas.

We shall now obtain an expression for the diffusion coefficient of an aerosol of relatively large size. Suppose this aerosol has charge e and moves in an electric field E. Its drift velocity is then $v = KE$, where K is the aerosol mobility. The force eE exerted by the electric field on the aerosol is then balanced by friction that can be described by the Stokes formula:

$$eE = 6\pi r_0 \eta v,$$

where r_0 is the aerosol radius and η is the gas viscosity.

Hence, we find that the aerosol mobility is

$$K = \frac{e}{6\pi r_0 \eta}. \tag{4.5}$$

Using the Einstein relation together with (4.5), we find that the aerosol diffusion coefficient is

$$\mathscr{D} = \frac{KT}{e} = \frac{T}{6\pi r_0 \eta}. \tag{4.6}$$

Since we have used the Stokes formula in deriving this expression, it will be valid for $r_0 \gg \lambda$, where λ is the mean free path of the gas molecules.

Substituting (4.6) in (4.4), we obtain the following expression for the aerosol aggregation rate constant:

$$k = \frac{8T}{3\eta} F(r_1, r_2), \quad F(r_1, r_2) = \frac{(r_1 + r_2)^2}{4 r_1 r_2}. \tag{4.7}$$

When $r_1 = r_2$, we have $F = 1$, but the result is not very different from unity when $r_1 \sim r_2$. For example, $F = 9/8$ when $r_1 = 2r_2$. Since the function F is not very sensitive to the ratio of the radii of the aggregating aerosols, we shall assume henceforth that the rate constant for the aggregation of two liquid aerosols is independent of their sizes. This will substantially simplify the results and the analysis.

Let us now write down the transport equation for the mass distribution $f(m, t)$ of the liquid aerosols, i.e., the Smoluchowski equation.[58] Since the coalescence of two aerosols of mass m and m' results in a new aerosol of mass $m + m'$, we write the Smoluchowski equation in the form

$$\frac{\partial f(m, t)}{\partial t} = -\nu f(m, t) + \nu \int_0^m f(m', t) f(m - m', t)\, \mathrm{d}m', \tag{4.8}$$

where the distribution function is normalized so that

$$\int_0^\infty f(m, t)\, \mathrm{d}m = 1, \quad \nu = Nk,$$

and N is the number of aerosols per unit volume. An important feature of this is that the aggregation rate constant is independent of the sizes of the aggregating aerosols and, consequently, of their masses.

It is interesting to consider the self-similar solution of this equation that is independent of the initial conditions and to which the system will tend in a time $t \gg 1/\nu$. It is clear from the structure of the equation that this solution is

$$f(m, t) = \frac{1}{\bar{m}} e^{-m/\bar{m}}, \tag{4.9}$$

where $\bar{m}(t) = \int m f(m, t)\mathrm{d}m$ is the mean aerosol mass at the given time. Substituting (4.9) in (4.8), we obtain

$$\frac{\mathrm{d}\bar{m}}{\mathrm{d}t} = \bar{m}\nu. \tag{4.10}$$

This equation enables us to etablish the function $\bar{m}(t)$ for arbitrary $\nu(\bar{m}, t)$. The latter function is determined by the dynamics of the gas containing the aerosols. In the simplest case of a stationary gas, the mass of the aerosol material per unit gas volume remains constant and this gives $N \sim 1/m$, i.e., $\nu \sim 1/\bar{m}$, so that the solution of (4.10) becomes

$$\bar{m} = m_0 N_0 k t, \quad \bar{m} \gg m_0, \tag{4.11}$$

where m_0 is the mean aerosol mass at the initial time and N_0 is the number of aerosols per unit volume at the initial time.

Like (4.9), the solution given by (4.11) is the asymptotic solution for $t \gg 1/\nu$. The initial conditions become "forgotten" after this time, and a self-consistent distribution independent of the initial conditions and admitting scaling is established.

This simple solution is possible because the aerosol aggregation rate constant is independent of the aerosol sizes and, consequently, of their masses.[7]

The equation given by (4.9) enables us to draw certain general conclusions about the dynamics of the above process, which should be valid for any law of aggregation of particles. Firstly, after a short time, the system "forgets" the initial conditions, i.e., it has an asymptotic distribution to which it tends independently of the initial conditions. Second, the size distribution function admits of scaling, i.e., there is a self-similar solution such that the distribution function can be reduced to a function of a single combination of the cluster size and time. The physics of the process shows that these conclusions should remain valid for different laws of aggregation of particles in the course of clusterization. We shall therefore use them as the starting point for estimating the validity of the results obtained by studying the dynamics of the evolution of fractal clusters.[60]

Basing ourselves on general ideas about the particle aggregation process, let us consider this process in relation to the evolution of a fractal cluster. In the above example, we were able to obtain a solution for the distribution function (4.9) for the aggregating particles because the aggregation rate constant was independent of the size of the colliding clusters. However, in general the aggregation rate constant is a function of the size of the colliding clusters, i.e.,

$$k \sim R^{2\omega}, \tag{4.12}$$

and this can be used to establish the relation between the parameter ω and the parameters describing the motion of clusters in space and their structure. This relation is[61]

$$2\omega = -\gamma + d - D_\omega, \tag{4.13}$$

where γ represents the dependence of the cluster diffusion coefficient on the cluster size ($\mathscr{D} \sim R^{-\gamma}$), d is the dimension of space, and D_ω is the fractal dimension characterizing the motion of clusters in space. We note that, in the case examined earlier, $\omega = 0$ for a compact system in three-dimensional space ($d = 3$), for Brownian motion of particles in space ($D_\omega = 2$), and for a diffusion coefficient inversely proportional to the particle size ($\mathscr{D} \sim 1/R$).

In the case of Brownian motion of clusters in space, (4.13) can be deduced directly from the diffusion equation (4.1). Actually, this equation leads to

$$k \sim \mathscr{D} R^{d-2} \sim R^{-\gamma+d-2},$$

which gives (4.13) in the form $2\omega = -\gamma + d - 2$ ($D_\omega = 2$ for Brownian motion).

The expression given by (4.13) enables us to deduce the scaling in the case of cluster-cluster aggregation. Actually, it then follows from (4.11) that the characteristic size and mass of clusters ($\bar{m} \sim R^D$) are given by[17]

$$R \sim t^{1/(D-2\omega)}, \quad \bar{m} \sim t^{D/(D-2\omega)}. \tag{4.14}$$

We can now use (4.13) to relate these parameters to the characteristics of cluster motion in space and the cluster fractal dimension.

More complete information on cluster aggregation follows from calculations in which this process was simulated by a computer. In particular, Fig. 9 shows the cluster size distributions at different instants of time, obtained in one of the first papers on cluster-cluster aggregation. Analysis of these distributions, using suitable statistics, leads to an overall picture of the dynamics of the cluster aggregation process for different assumptions about the parameters of this process. We shall now present the results of these calculations. We shall assume that the particle-size distribution function is

$$f(R, t) = Ct^{-w} R^{-\tau} F\left(\frac{R}{t^z}\right), \tag{4.15}$$

where $F(x)$ is a universal function that depends on the nature of the cluster encounter and coalescence. It follows from the normalization condition for the distribution function ($\int f R^{d-1} \mathrm{d}R = 1$) that the relation between the parameters is

$$z(d - \tau) - w = 0, \tag{4.16}$$

where d is the dimension of the space in which the process occurs.

Cluster aggregation dynamics has been investigated[62] in two-dimensional space on the assumption that the diffusion coefficient was independent of the cluster size ($\gamma = 0$). The motion of clusters in space was simulated in a standard

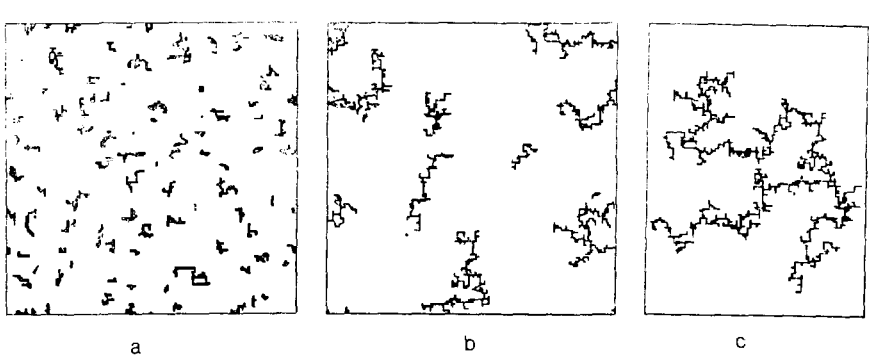

FIG. 9. Successive stages in the formation of a cluster (a–c) in the cluster-cluster model when all the particles simultaneously participate in the aggregation process.[7]

manner, i.e., a cluster was allowed to move by a lattice constant in any direction according to the Monte Carlo method. Collisions between clusters leads to their coalescence.

The more general case, where the cluster diffusion coefficient is a function of the cluster size ($\mathscr{D} \sim R^{-\gamma}$), has also been considered.[63] We note that (4.9) corresponds to $\gamma = 1$ for liquid aerosols and, according to this formula, $z = 0.5$. According to the results published in Ref. 63, the aggregation of fractal clusters in three-dimensional space in this case corresponds to $z = 0.8$, while (4.14) gives $z = 0.6$. We must now consider one further peculiarity of the distribution function. The expression given by (4.9) corresponds to the situation where there are always more small clusters than large clusters, although the number of the former decreases with time. This conclusion is also valid for the aggregation of fractal clusters[62] if their diffusion coefficient is independent of their size. However, when the cluster diffusion coefficient decreases with increasing cluster size, and this variation is rapid enough, small clusters vanish at a much greater rate than the rate of breakup of larger clusters. The distribution function (4.15) is then no longer monotonic, i.e., its maximum value occurs at nonzero argument. It was found in Ref. 63 that the transition from the one form to the other occurred in the two-dimensional case for $\gamma = 0.25$ and, in the three-dimensional case, for $\gamma = 0.5$.

The above method of studying the cluster-size distribution function can be summarized as follows. A large number of particles is simultaneously let into the space in which they execute Brownian motion and undergo clusterization So long as the number of clusters in the system is large, their particle-number distribution at each instant of time is represented by a distribution function that depends on the number of particles and on time. Repetition of this operation improves the precision of the distribution function obtained in this way. Analysis of the results obtained by this method and also from the Smoluchowski equation can be used to determine the scaling in this process.

In the case of cluster-particle aggregation, scaling can be established more simply.[64] The rate of change of the number of particles in a cluster is

$$\frac{dN}{dt} = J,$$

where the particle flux to the cluster is given by (4.1), i.e., $J \sim \mathscr{D} n_0 R^{d-2}$, where n_0 is the free-particle density well away from the cluster and d is the dimension of the space. It follows that, since the number of particles in the cluster is related to its size by $N \sim R^D$, we find that the time dependence of the cluster size is

$$R^\alpha \sim t, \quad \alpha = D - (d - 2). \tag{4.17}$$

In particular, in three-dimensional space, we have $\alpha = 1.5$.[8)] Analysis[65] shows that there is a critical cluster growth rate that is limited by the density of particles in the cluster penetration zone. If the cluster growth rate exceeds the critical value, the character of the cluster growth is found to change, and there is a corresponding change in its structure.

When the cluster-cluster aggregation process was investigated, we assumed that the resulting clusters satisfied the gas condition, i.e., the volume per cluster was much greater than the volume actually occupied by each cluster. However, since, as the cluster size increases, the mean density of matter within the cluster decreases, the gas condition will be violated at some stage in the process. We shall then obtain a set of fractal clusters with mean separation comparable with the cluster size. The subsequent cluster aggregation process leads to the formation of one large cluster. This stage simulates the process of gel formation (solidification of a colloidal mass in solution), i.e., the process of transition from sol to gel. The gel formation process is very specific,[66,67] and the resulting cluster has a higher fractal dimension as compared with the case where the gas condition is satisfied for the aggregating clusters.

We note one particular feature of aggregation of solid particles in a gaseous plasma system. In the case when the initial high density of particles is produced by evaporation of material acted upon by an electric current aerosols of cylindrical shape are formed from the solidifying aerosols at the initial stage of relaxation of the vapor produced. Such a process occurs in the presence of electric fields in the system. To demonstrate this assertion we have included Fig. 10 which reflects the nature of the interactions of a cylindrical and a spherical aerosol in a uniform electric field when charges are induced on the aerosols by this field which bring about this interaction. It can be seen that in the aggregation of cylindrical and spherical aerosols it is more advantageous for the spherical aerosol to approach the end face of the cylindrical one. Therefore the aggregation of aerosols in a strong electric field favors the growth specifically of cylindrical aerosols.

We now note one specific example corresponding to the real situation. Suppose that the radii of spherical and cylindrical aerosols are 1μ, and the length of a cylindrical aerosol is greater by a factor of 100. Suppose a spherical aerosol lies on the continuation of the axis of a cylindrical aerosol at a distance of 10 radii from its end. The energy of attraction between the aerosols due to the interaction between the induced charges will then be equal to the mean thermal energy of a gas particle at room temperature in an electric field of less than 200 V/cm.

This example confirms that, in the initial stage of aggregation of solid aerosols, the evolving structures are cylindrical in shape. This is well-known in the physics of aerosols,[57,59,68] where such systems are called chained aggregates. It is known that these chained aggregates are formed when aerosols are produced by the electric method. As an example, we note the 50-year old experiment[69] in which is was shown that magnesium oxide smoke, produced in an arc discharge, contained chained aggregates, whereas the smoke produced by burning a magnesium foil consisted of magnesium oxide particles of compact structure.

The formation of chained aggregates during the first stage of aerosol aggregation facilitates the evolution during the following stage of looser clusters than would be obtained from the aggregation of compact aerosols. This must therefore be taken into account in the analysis of the aggregation of aerosols formed after the evaporation of material in an arc discharge, during the explosion of wires, under the influence

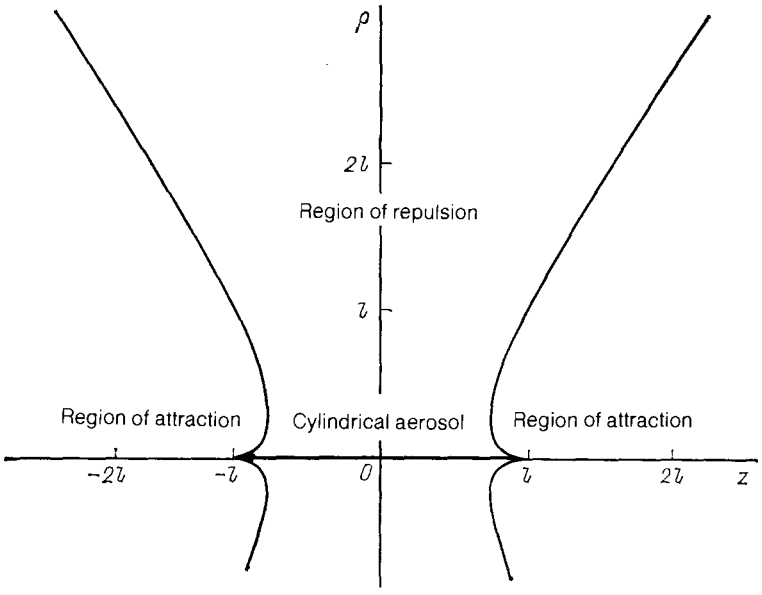

FIG. 10. Nature of the interaction of a chained aggregate with a spherical aerosol in a uniform electric field.

of lightning or a pulsed discharge, and other electrically induced events.

When cluster-cluster aggregation was examined, the analysis was confined to the case where the initial mass of particles in a given volume did not change with time. However, real gas-dynamic conditions may result in the nonconservation of the mass of particles in a given volume. One such possibility was discussed in Ref. 70. New simple particles were constantly fed into the volume, the rate of supply per unit volume per unit time being k. The number of clusters in the system is then given by

$$N(t) \sim k^{\alpha} f(k^{\beta} t),$$

where[37] $\alpha + \beta = 1$ and the asymptotic expressions for the required functions are

$$f(x) = \begin{cases} x, & x \ll 1, \\ 1, & x \gg 1. \end{cases}$$

Actually, during the first stage, the number of clusters in the system is proportional to the number of simple particles within it, but the system eventually reaches saturation. The dependence of the diffusion coefficient on cluster size is then found to affect only the tail of the distribution function, which does not really affect its normalization. The required parameters in three-dimensional space were found to be[70] $\alpha = 0.47 \pm 0.05, \beta = 0.54 \pm 0.05$.

A more complicated model that included the aggregation of clusters and evaporation of particles was examined in Ref. 71. In the presence of these processes a cluster cloud was generated in two-dimensional space from a compact formation. Over a long period of time, the cloud could be desorbed by an exponential cluster-size distribution and the same fractal dimension of the clusters. When the cluster motion was diffusion-limited, their fractal dimension was close to unity, whereas for clusters moving along rectilinear trajectories the fractal dimension was close to 4/3.

The information that has been obtained on the dynamics of aerosol aggregation provides us with a good picture of this process, which can be used in the qualitative and quantitative analysis of such phenomena.

5. FRACTAL CLUSTERS IN PHYSICAL PROCESSES AND PHENOMENA

We shall now examine some special cases of fractal clusters observed experimentally, and also studies of processes and phenomena affected by the fractal structure of such clusters. Although the number of such examples is limited at present, experience shows that an understanding of the nature of fractal clusters helps in finding new areas in which these entities may be useful. The study of films on surfaces occupies a prime position among experimental studies of fractal structures. When a film is produced by depositing solid aerosols on a surface, it takes the form of a fractal cluster if the aerosol and substrate are appropriately chosen. This occurs when the aerosols are loosely bound to the substrate, but bind strongly to one another. A surface fractal cluster can arise from a volume cluster deposited on a surface.

There have been many studies of surface fractal clusters. One of the first was due to Forrest and Witten.[74] By analyzing the photograph of metal-particle aggregates in air, recorded in an electron microscope, they discovered the fractal structure of these systems. The usual cluster photograph covered an area of a few square microns and contained part of a cluster with a large number of particles. A grid was used to divide the photograph into cells, and, depending on the degree of occupation of these individual cells, they were regarded as filled or empty. The data obtained from the photograph were then stored in numerical form in a computer (zeros and units) and analyzed. The fractal dimension of the clusters was determined from the distance dependence of the correlation function (2.3), or from the number of occupied cells as a function of the area of a defined portion of the photograph. The results are listed in Table V. The fractal

TABLE V. Fractal dimension of clusters formed after evaporation of a material.

material	Fe	Fe	Zn	Zn	SiO_2
D_α	1.69±0.02	1.68±0.01	1.67±0.02	1.68±0.02	1.55±0.02
D_β	1.52±0.04	1.56±0.02	1.50±0.04	1.60±0.04	1.55±0.06

dimension of the clusters, averaged over these data, is 1.60 ± 0.07. The approach used in this study formed the basis for the Witten-Sander model,[1] which took research into fractal clusters to a new level of sophistication.

Another example of an experimental study of a fractal cluster is given in Ref. 75. Gold particles were produced by the reduction of $Na(AuCl_4)$ by tri-sodium citrate. Spherical gold particles, 14.5 mm in diameter, were formed during the first stage.[9] This was due to the fact that the surface-adsorbed citrate ion caused the gold particles to be charged, which ensured that the surface of a particle repelled atomic gold ions and prevented further growth of the particles. The addition of a small amount of pyridine to the solution removed the surface charge on the particles and initiated the aggregation process. Individual gold particles were thus found to form clusters, and these were investigated in Ref. 75. The clusters were deposited on a grid and then photographed in an electron microscope. The photographs were examined to determine the number N of particles as a function of the cluster size L. Since the optical thickness of the cluster was small, this relationship could be determined with good precision. Analysis of 100 clusters on the grid ($L \sim 1$ μm) showed that the fractal dimension was $D = 1.77 \pm 0.1$ (Fig. 11). To within experimental precision, the mass of the cluster formed in this way could be approximated by

$$m = m_0 \left(\frac{R}{a}\right)^D, \tag{5.1}$$

where $m_0 = 3 \times 10^{-17}$ g is the mass of an individual particle, a is its radius, and R is the radius of the cluster.

Another example of a fractal cluster is shown in Fig. 12, taken from Ref. 76. This was a film of $NbGe_2$ on a quartz substrate. During the experiment, the substrate was heated to 840 °C, with a mixture of helium and germanium vapor above it, the total gas pressure being less than 0.1 Torr. High-frequency spraying of niobium into the gas mixture was then performed. The interaction between niobium and germanium resulted in the formation of aerosols in the form of a chemical compound of these two components. As they settled down on the substrate, these aerosols produced a film in the form of fractal clusters. The film thickness was 0.2–0.5 μm, the size of fine grains was 0.1 μm, and the size of large grains formed on the cluster periphery was about 1 μm.

Analysis of the observed surface clusters yielded the fractal dimension $D = 1.88 \pm 0.06$. When the thicker ends of the clusters were excluded, the fractal dimension fell to $D = 1.73 \pm 0.08$, which agreed with the Witten-Sander model[1] to within the experimental uncertainty. Calculations show that the formation of these clusters can be described by the Witten-Sander model if a two-stage scheme is adopted. During the first stage, the probability of attachment of a particle to a cluster on contact is equal to unity, and this results in a cluster with fractal dimension of about 1.7. An approximately equal number of individual particles takes part in the second stage. The probability of attachment to the cluster is now assumed to be 0.1 and this leads to thicker cluster branches and a higher fractal dimension. The cluster structure obtained in this model agrees with observations. This shows that the actual cluster formation process is quite complicated.

We note that in the last two cases the *surface* cluster-formation model was used to describe the experimental results. However, in the first case (and, possibly, in the second, too), the formation of the cluster occurred in space, so that the fractal dimension deduced from these data was closer to the three-dimensional case. The observed fractal cluster is then better represented by the cl-cl model which, in the

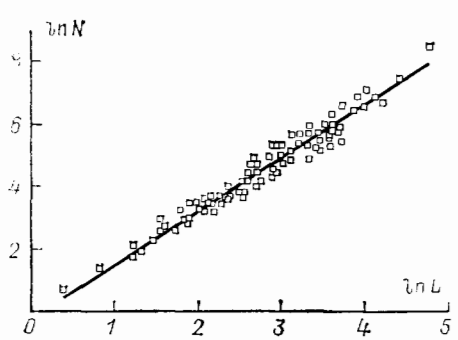

FIG. 11. Mass of colloidal cluster of gold particles as a function of its size.[75] The mass of the cluster is expressed in units of 10^{-17} g and its size in terms of the size of the individual particles (14.5 nm). The straight line corresponds to the fractal dimension $D = 1.75$.

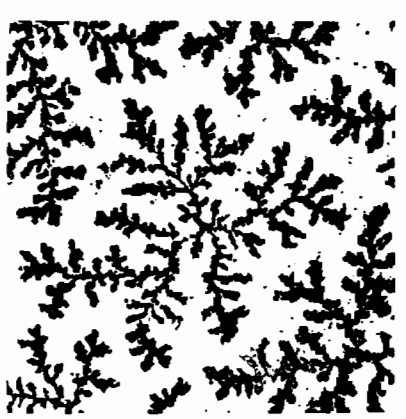

FIG. 12. Surface cluster of $NbGe_2$ formed on a quartz substrate.[76]

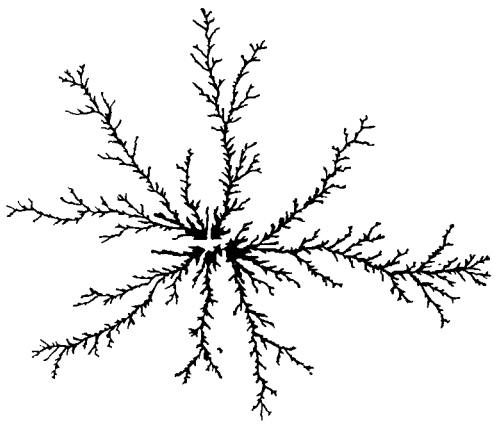

FIG. 13. Fractal cluster formed by depositing zinc on a surface by electrolysis.[77] The fractal dimension of the cluster is 1.66 ± 0.03.

three-dimensional case, corresponds to the fractal dimension $D = 1.77 \pm 0.03$ (see Table III).

Another example of an observed surface fractal cluster is reported in Ref. 77. The substrate employed also serves as an electrode placed in an electrolyte, and the application of a potential difference between electrodes results in the deposition of a metal (zinc). So long as the potential difference between the electrodes does not exceed a certain critical value, zinc is deposited onto the substrate in the form of fractal clusters of fractal dimension 1.66 ± 0.03 (Fig. 13), which is in agreement with the Witten-Sander model. When the potential difference is increased above the critical value, the result is a change in the nature of the deposition of metal particles on the substrate and an increase in the fractal dimension of the resulting cluster.

In all the cases examined above, the clusters were investigated by analyzing their photographs recorded in an electron microscope. This method can be used to study two-dimensional clusters formed on a substrate, or the projections of three-dimensional clusters on a plane. A convenient diagnostic method, suitable for three-dimensional clusters, was used in Refs. 78 and 79, where x-ray scattering by the clusters was employed. The x-ray intensity scattered by a fractal cluster is proportional to the Fourier component of the density of the material within the cluster and, according to (2.2)–(2.4), we obtain

$$S(k) \sim k^{-D_\alpha}, \tag{5.2}$$

where S is the scattered intensity and k is the photon wave vector. This relation is valid for $1/R \ll k \ll 1/a$, where R is the size of the cluster and a the size of an individual particle. Hence, by measuring the scattered intensity as a function of wavelength, it is possible to determine the fractal dimension D_α of the cluster.

The formation of colloids from silicon dioxide was investigated in Ref. 78. As in the above example of gold particles, the parameters of the solution were chosen so that particles of strictly defined size (2.7 nm) were formed. Their subsequent growth was brought to an end by the appearance of a charge on their surface. This prevented the attachment of further molecules of silicon dioxide, which eventually formed other particles of the same size. The acidity of the solution was then altered, and this allowed the particles to aggregate. By measuring the scattered x-ray intensity for different wavelengths, it was possible to show that the aggregation of these particles resulted in a cluster of fractal dimension $D_\alpha = 2.12 \pm 0.05$.

Another example investigated by x-ray diagnostics was the formation of silicon dioxide polymers in nonaqueous solutions.[79] These polymers have a branched structure, and the fractal dimension deduced from x-ray scattering by these polymers is $D_\alpha = 2.0 \pm 0.1$.

As can be seen, the fractal dimension obtained in the above two three-dimensional clusters was very similar, and turned out to be greater than the fractal dimension of clusters in the cl-cl model, but smaller than that in the Witten-Sander model. This suggests a complex cluster formation process, so that a more detailed investigation of the aggregation mechanism is necessary. The fractal dimension of the resulting clusters is best described by the rectilinear trajectory model and cl-cl aggregation (see Table II), which can be valid only for large clusters when cluster diffusion is of no significance in relation to their displacements.

The aggregation of solid particles in three dimensions, or on a surface, is the most common mode of formation of fractal clusters. However, additional analysis is necessary if the fractal structure of the resulting clusters is to be determined. Because of the absence of this type of analysis, our review does not cover observations of objects that *may* have had fractal structure. For example, loose structures were produced in Ref. 80 by exploding metal wires for certain parameters of the current flowing through the wires, and these structures were referred to as filamentary. By analogy with processes producing fractal clusters, these structures can probably be classified as fractal clusters but, owing to the absence of the necessary analysis, this identification must be regarded as tentative.

Fractal clusters are efficiently produced as a result of the aggregation of aerosols in space or on a surface, provided definite conditions are observed. The clusters subsequently aggregate, and this destroys their fractal structure. Fractal clusters are therefore not observed in situations where they could be expected. The physical descriptions of these structures that have appeared in recent years will undoubtedly assist in the more detailed study of many real processes accompanied by the aggregation of aerosols.

In addition to the formation of fractal clusters from solid aerosols in space and on a surface, there are also other processes and phenomena in which the concept of the fractal structure of clusters is useful. Let us consider some of them. Figure 14 shows the Lichtenberg figures, which represent the dielectric breakdown pattern in a gaseous, liquid, or solid insulator. In the experiment performed in Ref. 81, one of the electrodes was at the center and the other was in the form of a ring on a dielectric surface (see also Fig. 7). The bright areas of the dielectric, over which the breakdown current flows, resemble a fractal cluster. Its fractal dimension, determined from the relation between the cluster size and the number of elements, is about 1.7. Because of limited resolution, it is not

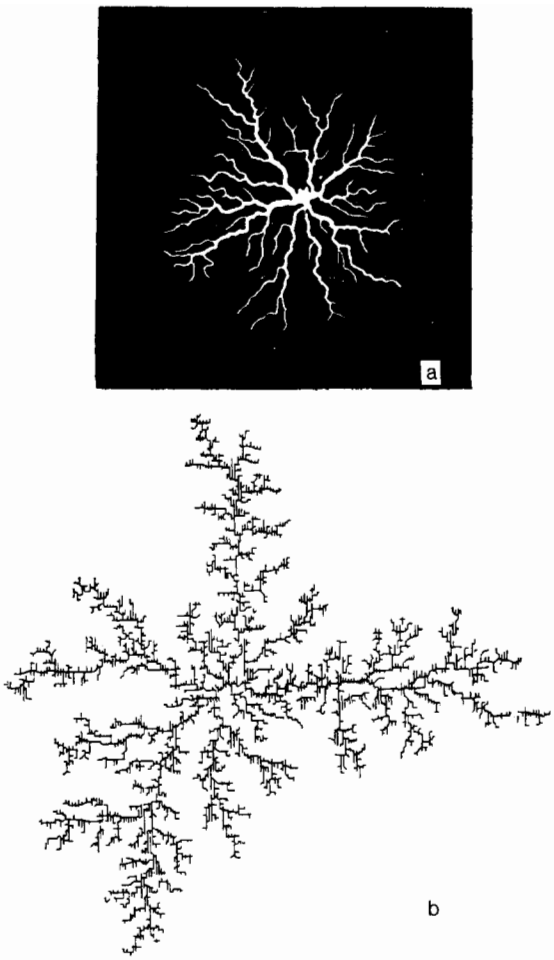

FIG. 14. a—Lichtenberg figure[81] (emission intensity from a dielectric breakdown, integrated with respect to time) for a glass plate in sulfur hexafluoride gas at a pressure of 0.3 MPa; b—pattern obtained[81] by simulating the process by the Monte Carlo method in a computer. The fractal dimension of the cluster is 1.75 ± 0.02.

possible to determine this quantity from the correlation between element densities. The simplest model of this discharge, which includes the motion of the bright point over broken lines with given straight-segment length, yields $D = 1.75 \pm 0.02$ for the fractal dimension of the Lichtenberg figure.

Another example[82] involves hydrodynamics. When a low-viscosity liquid (e.g., water) is forced through a high-viscosity liquid (e.g., oil), the so-called viscous fingering instability is found to set in. The distribution in space of the low-viscosity liquid then acquires a branched structure that can be approximated by the structure of a fractal cluster.

The next example refers to the adsorption of molecules by the internal surface of porous materials.[83–87] It turns out that the pore size distribution is given by (2.3). Hence, the porous material is characterized not by its porosity, which is largely determined by the pore size, but by the fractal dimension of the medium that describes the pore distribution. This is why, as confirmed by analyses of adsorption properties of individual porous materials for different molecules, the total specific size of an absorbing surface as a function of the size of absorbed molecules can be represented by the formula for a fractal system.[86]

If we consider the system of voids in a porous material as a fractal cluster, its fractal properties can be determined from (5.2), using x-ray or neutron scattering data. This was used in Ref. 85 to show that the fractal dimension of lignite was 2.56 ± 0.03. The fractal properties of porous sandstone were investigated in Ref. 87. The scattering of secondary electrons in a scanning electron microscope was used to show that the fractal dimension of different samples of sandstone was 2.57–2.87, the porosity being 5–30%. Moreover, the self-similarity of individual portions of the specimens, and the fractal property defined by a formula such as (2.3), were found to be valid for regions whose sizes differed by 3–4 orders of magnitude (from 0.1 to 100 μm).

The above examples show that the concepts of fractal clusters and fractal structures extend our knowledge of many systems and phenomena, and facilitate a more detailed analysis of real processes and phenomena. These concepts provide the foundation for the successful development of experimental studies of fractal structures and of the dynamics of their formation.

6. FRACTAL CLUSTERS AND BALL LIGHTNING

Fractal clusters are of direct relevance to ball lightning. Practically the only model of ball lightning capable of explaining its constant shape and size in the course of its evolution is at present based on the hypothesis that the active material of ball lightning is a cluster of filamentary aerosols.[89] This model is based on experimental studies[80] of the relaxation of metal vapor, in which systems consisting of clusters of filaments have been observed. In view of the considerable interest in the phenomenon of ball lightning, let us examine this question in greater detail. There is now a sufficient number of reviews and books[90–103] that have collected together and analyzed available experimental data on ball lightning and that examine possible models of the phenomenon. There is a relatively large number of observations of ball lightning. For example, in his book, Stakhanov[100] has examined over 1000 cases of ball lightning observed in the USSR, whereas Barry's book[102] covers over 1800 scientific publications reporting observations of ball and bead lightning, and analyzes experimental data and models of ball lightning. The information on ball lightning that has now accumulated leads to the unambiguous conclusion that the phenomenon does actually occur, and enables us to construct a picture of a typical ball lightning with averaged parameters. The parameters of such a ball lightning are listed in Table VI.

When models of ball lightning are analyzed, it is important to consider five aspects of this phenomenon that must be independently incorporated in the description of the model. First, we have to consider how energy is stored in ball lightning, second, the nature of heat release in ball lightning, third, the shape of ball lightning and the structure of its active material, fourth, the mechanism responsible for the emission of radiation from ball lightning, and, fifth, the elec-

TABLE VI. Parameters of the average ball lightning based on observational data.[103]

Parameter	Value or conclusion
1. Diameter, cm	28 ± 4
2. Lifetime, s	$10^{0.95 \pm 0.25}$
3. Speed, m/s	4 ± 1
4. Energy of ball lightning, J	$10^{4.3 \pm 0.2}$
5. Energy density in ball lightning, J/cm^3	$10^{1.2 \pm 0.4}$
6. Luminous flux	1400^{+800}_{-600}
7. Color	White ($24 \pm 2\%$), yellow ($24 \pm 2\%$), red ($18 \pm 2\%$), orange ($14 \pm 2\%$), blue and violet ($12 \pm 1\%$), and so on.*
8. Correlation with electrical phenomena in the atmosphere	$70 \pm 10\%$ of ball lightning events are observed in stormy weather
9. Disintegration of ball lightning	$50 \pm 20\%$ of all cases, with ball lightning involving an explosion
10. Probability of appearance of ball lightning, km^{-2}min^{-1}	$10^{-8.5 \pm 0.5}$

*Figure in parentheses shows the relative probability of observing a ball lightning of the given color.

tical phenomena occurring in ball lightning. If we assume that there are no external sources of energy for the ball lightning, analysis of the processes occurring within it[104] leads to the conclusion that the only way in which energy can be stored in ball lightning is by some chemical mechanism. Indeed, the lifetime of ball lightning is much longer than the typical times of elementary processes involving collisions between particles in air, and is sufficient for the internal energy of the hypothetical ball lightning to be converted into heat. For example, in a system containing plasma or excited atoms or molecules of sufficient energy, the recombination of charged particles or the quenching of excited states occurs in a time much shorter than the observed lifetime of ball lightning. A chemical reaction involving sub-barrier transitions of nuclei can take a long enough time so as not to impose this restriction on the chemical method of energy storage.

If we now concentrate our attention on the chemical method of energy storage in ball lightning, we must emphasize that there is a special chemically active component in air, namely, ozone. Ozone is readily produced by different methods of excitation of air, with higher concentration than other chemically active components.[105,106] It dissociates quite slowly in air at moderate temperatures.[107] Ozone can therefore be one of the chemical components of the active material in ball lightning in which it acts as an oxidizing agent.

We now turn to the second of the above five aspects of the ball-lightning phenomenon, namely, the nature of heat release. Heat is released as a result of chemical processes, and the emission of radiation is a side effect of this. Analysis[107] shows that chemical transformations occur with maximum probability in a gaseous heterogeneous system. The gas component (ozone) enters the heterogeneous system very slowly, so that in the most likely situation, the gas and the heterogeneous systems are superimposed from the start. One way of doing this is to have a heterogeneous system with a porous structure in which the gas component is adsorbed by internal surfaces.[10]

The essential requirement that the heat release in ball lightning must satisfy is that it must be an intensive and slow process. The former means that the specific energy release must be high enough and capable of producing sufficient heating of the active material in the ball lightning. This, and the requirement that the process be slow, follows from the observed parameters of ball lightning (see Table VI). However, there are problems with satisfying both requirements at the same time. In fact, we shall show that they *cannot* be simultaneously satisfied in a simple heat-release process, i.e., a single-stage process. Thus, the characteristic time constant τ of a chemical process is related to the temperature T of the reacting components by the Arrhenius law:

$$\frac{1}{\tau} = \frac{1}{\tau_0} e^{-E_a/T}. \tag{6.1}$$

If we take the characteristic time in the pre-exponential factor to be the collision time between bound molecules, i.e., $\tau_0 \sim 10^{-13}$–10^{-12} s and, if we demand that, at room temperature, the time taken by the process must be of the order of the lifetime of ball lightning ($\tau \sim 10$ s), we find that the activation energy for the process is $E_a = 18$ kcal/mol. This is a reasonable figure because it falls into the range of existing values of activation energy for chemical processes. If we use this value, we find that $\tau = 0.004$ s at $T = 400$ K, i.e., an increase in temperature by 100 K produces an increase in the rate of the process by a factor of several thousand. This means that, if there is a possibility that the temperature will change, the process cannot be slow.

It is clear that this conclusion does not depend on the numerical parameters that we have used. It is a consequence of the fact that the time for the process (6.1) is a rapidly-varying function of temperature which, in turn, is determined by the considerable difference between the typical molecular time τ_0 and the typical time τ for the process, i.e., the lifetime of ball lightning. The heat-release process in which we are interested cannot therefore be both intensive and slow if it is a single-stage process. The question then arises whether there is some process that is both intensive and slow. Experimental studies[108,109] have revealed an ex-

TABLE VII. Duration of the slow stages of the process defined by (6.2).

T, K	300	400	500	600	700
$\frac{1}{\nu}$, c	330	190	140	110	90
$\frac{1}{\omega}$, c	740	170	70	40	26

ample of this, namely, the burning of charcoal dust in ozone absorbed by it, which can be described phenomenologically as follows:

$$C \ldots O_3 \xrightarrow{t_s} X \xrightarrow{\nu} Y \xrightarrow{1/\tau} Z \xrightarrow{\omega} CO_2,\ CO\,. \quad (6.2)$$

The rates of the different stages of the process are indicated above the arrows, and the times of the slowest stages are listed in Table VII. Combustion thus consumes $89 \pm 3\%$ of the dust, and the heat released by the entire weight of dust is 28 ± 3 kJ/g, i.e., it is comparable with the specific heat release in the complete combustion of carbon in oxygen (32 kJ/g). The main by product of the process is CO_2 ($84 \pm 5\%$ at the saturation temperature of 226 K[110]). Another feature of the process is the ozone saturation temperature memory of the specimen. When the ozone saturation temperature is less than 245 K, subsequent processes are determined by (6.2). However, if ozone saturation occurs above 245 K, subsequent heating of the specimen results in the decomposition of ozone to oxygen, and the charcoal is preserved intact. Apparently, the absorption of ozone by charcoal is accompanied by a number of chemical changes on its internal surface, which depend on the temperature of the process, and this determines the subsequent evolution of the system.

It follows that (6.2) may be looked upon as a model process for ball lightning. The above investigations enable us to answer questions relating to the first two aspects of ball lightning, i.e., energy storage and heat release. We shall now concentrate on the first aspect, which is directly related to the theme of our review.

Observed facts relating to ball lightning impose a number of conditions on the ball lightning model, which turn out to be mutually contradictory for most hypotheses about the nature of ball lightning. In particular, heat release in chemical processes gives rise to convective flows which modify the region occupied by the active material when the latter is present in the form of gas or dust. Estimates[111] show that the heating of the active region in atmospheric air by an amount of the order of 100 K results in loss of shape and change of size in a time shorter than 0.1 s, which is much shorter than the observed lifetime of ball lightning. This means that the active medium in ball lightning cannot be dust or gas.

The hypothesis of filamentary structure of the active medium in ball lightning[89] is not in conflict with the above conditions. However, the aggregation of solid aerosols results in a fractal-cluster structure and not a filamentary structure. We shall therefore assume that the active material of ball lightning does, in fact, have a fractal structure. This more detailed representation of the structure is not of fundamental significance for many processes but, in other cases, it provides us with a more complete picture of the system. The essential point then is that the fractal cluster is the only structure that produces a light and stiff configuration of the active medium. So long as the structure is not destroyed in the course of chemical processes, the ball lightning will retain its shape. The electrical charge carried by ball lightning prevents the "collapse" of the structure.[89] We shall now consider the consequences that ensue from the hypothesis of fractal structure of the active medium of ball lightning.

One of them is the motion of heated air, which creates the lifting force for the structure. The motion of heated air above the system is equivalent to motion out of a tube. This problem was examined by Ya. D. Zel'dovich[112,113] and we shall use the results obtained by him. The heated air rises above the heated body into an expanding cone. Its directed velocity in the region occupied by the structure is given by the following order-of-magnitude expression:

$$u \sim \left(gR_0 \frac{\Delta T}{T}\right)^{1/2}, \quad (6.3)$$

where g is the acceleration of gravity, R_0 is the radius of the system, ΔT is the temperature difference between the system and the temperature of ambient air, and T_0 is the ambient air temperature ($\Delta T \lesssim T_0$). Typically, $u \sim 1$ m/s for $R_0 \sim 10$ cm, so that the Reynolds number is $\mathrm{Re} \sim R_0 u/\nu \sim 10^3$–$10^4$ (ν is the kinematic viscosity of air) and the force of resistance to the motion of the structure in air is

$$\mathcal{F} \sim \rho u^2 S,$$

where ρ is the mass density of air and S the cross section of the structure, i.e., the projected area of the system on a plane perpendicular to the direction of motion. The steady-state motion of air thus produces the lifting force

$$F = a\rho g R_0 \frac{\Delta T}{T} S, \quad (6.4)$$

where a is a numerical factor. If the lifting force balances the weight of the structure, the ball lightning will float in air.

The numerical factor a in (6.4) has been determined in a series of simulation experiments.[114] Lumps of metal, 0.8–2 cm in radius and weighing 20–150 mg, were prepared from tungsten wire of radius 4 and 7 μm. The metal pieces were suspended on the end of a thin quartz filament cantilever, and the deflection was used to determine the force due to the metal. The lump was then heated by laser radiation and its temperature was determined from the thermal radiation it emitted. Simultaneous measurements of the temperature of the metal lump and the lifting force were used to determine a in (6.4). The result was $a = 11 \pm 5$. Hence, it follows that ball lightning can float even when it contains a substantial amount of matter in the structure. Using this value of the numerical factor in (6.4), we find that the condition that an optically opaque fractal cluster ($D > 2$) will float is

$$\frac{m}{M} = 8\,\frac{\Delta T}{T_0}. \quad (6.5)$$

For an optically thin ($D < 2$) fractal cluster, this condition is

$$\frac{r_0}{R_0} = 5\,\frac{\rho}{\rho_{cl}}\,\frac{\Delta T}{T_0}; \quad (6.6)$$

where m is the mass of the fractal cluster, M is the mass of air in its interior, ρ is the density of air, and ρ_{cl} is the density of the cluster material.

A further important feature of the air dynamics in this phenomenon is that the motion of air takes up a considerable fraction of the released energy. Indeed, the power expended in heating the flowing air is $\mathscr{P} \sim \rho c_p \Delta T \cdot u \pi R_0^2$, where c_p is the specific heat of air. Hence, we find that the power expended per unit volume of the structure is

$$\frac{\mathscr{P}}{V} = p_0 \left(\frac{\Delta T}{T_0}\right)^{3/2}, \tag{6.7}$$

where $p_0 \sim \rho_0 T_0 c_p (g/R_0)^{1/2}$. Substituting numerical values for the coefficients in this formula, we find that $p_0 = 7.2$ W/cm^3 for $R_0 = 10$ cm. This result leads us to the conclusion that ball lightning must contain a large amount of energy per unit volume.

The fractal structure of ball lightning thus leads to consequences that are due to its gas dynamics. Moreover, it is important to note that we started with the assumptions that the heat release was time-independent and the ball lightning was located well away from all surfaces. These assumptions are not valid in practice, so that the above picture is only qualitatively correct.

We now turn to the fourth of the above aspects, i.e., the emission of radiation by ball lightning. We first consider the thermal radiation emitted by the body of ball lightning as it is heated by chemical reactions, although it is clear that this radiation will not explain all the observed colors (see Table VI). If the sizes of particles within the body of the ball lightning are small in comparison with wavelength, infrared emission will be suppressed to some extent. However, this effect has no fundamental influence on the thermal-emission picture of the fractal cluster.

Nevertheless, the emission of thermal radiation can explain one type of ball lightning, i.e., that produced from metal vapor as it cools. The first stage is the formation of liquid aerosols which grow in the vapor, solidify, and eventually combine into fractal clusters. We shall assume that the optical thickness of the cluster is small and that it consists of a set of cylindrical filaments. In accordance with the theory of thermal emission by a metal surface,[115] the power radiated per unit area is proportional to $T^{9/2}$, where T is the surface temperature. Assuming that the rate of loss of energy by the system is determined by the emission of radiation by the surface, we find that the characteristic cooling time τ_0 is proportional to the filament radius. Table VIII lists values of the required parameter $\tau_0 = T/(\mathrm{d}T/\mathrm{d}t)$ for metal filaments, $10\,\mu$m in radius. Analysis of the data listed in the table shows that this is a possible mechanism. It can explain the glowing beads that are sometimes observed when a wire is shorted or explodes. Such glowing beads usually fall to the ground, and are extinguished. However, the scheme that we have proposed will not explain most of the observed cases of ball lightning because, usually, the lifetime of ball lightning is much longer (see Table I). When we analyze the general case of emission with a view to gaining some idea about the brightness of ball lightning, we shall make two estimates by comparing the average ball lightning with a blackbody source. First, let us find the temperature of a perfect blackbody of radius equal to that of the average ball lightning, which produces the same luminous flux as the ball lightning (see Table VI). The result is $T = 1360 \pm 30$ K. Second, let us find the temperature of a perfect blackbody that would ensure the same luminous efficiency[11)] as the average ball lightning (according to Table VI, the luminous efficiency of the average ball lightning is $10^{-0.2 \pm 0.65}$ cm/W, the luminous efficiency of an electric lamp is 14 cm/W). This temperature turns out to be 1800 ± 300 K. The effective temperature of the radiating particles is higher than these figures would suggest because, in the former case, the emission of radiation by ball lightning is confined to a narrow part of the spectrum and, in the latter, most of the energy lost by the ball lightning is taken up by gas-dynamic motion. One would therefore expect that the effective temperature of radiating particles in ball lightning is $T \gtrsim 2000$ K.

An important feature of the emission processes in atmospheric air is the high rate of quenching of the radiating atoms and molecules by air molecules. For example, the rate of quenching of resonantly excited sodium atoms Na($3p$) by nitrogen molecules is $(7.0 \pm 1.5) \times 10^{-10}$ cm^3/s at temperatures between 400 and 2200 K, whereas the corresponding rate for quenching by oxygen molecules at 1000–2500 K is $(12 \pm 1) \times 10^{-10}$ cm^3/s. These data are taken from the review of Ref. 117 and the indicated uncertainties correspond to the statistical averaging of the results reported by different workers. If we use these data, we find that, at atmospheric pressure and 2000 K, the probability that a resonantly excited nitrogen atom will be quenched in air is 0.98, whereas the probability of quenching by emission is 0.02.

The high quenching probability obtained for excited atoms and molecules in atmospheric air means that they are in thermodynamic equilibrium with the air, and their local density does not depend on the way they are produced. When taken together with the restricted local temperature in

TABLE VIII. Radiative cooling time for filaments of radius $10\,\mu$m.

T, K		1200	1400	1600	1800
τ_0, c	Copper	2.8	—	—	—
	Iron	1.3	0.74	0.46	0.31
Fraction of emission in the optical part of the spectrum		$1.6 \cdot 10^{-4}$	$9.1 \cdot 10^{-4}$	$3.2 \cdot 10^{-3}$	$7.9 \cdot 10^{-3}$

ball lightning, this fact enables us to identify the excited atoms and molecules that could be responsible for the emission of radiation by ball lightning. The necessary excited states must have short radiative lifetimes, they must take part in radiative transitions to the ground state, and the photons created in this way must lie in the optical part of the spectrum. Excited atoms or molecules that could produce the required emission by ball lightning are shown in the diagram of Fig. 15.

The above mechanism of ball lightning is similar to the emission of radiation by a flame into which some material has been added, or the radiation emitted by the illuminant mixture in pyrotechnics. Let us therefore analyze from the standpoint of emission by a yellow ball lightning, the radiation emitted by the yellow-flame mixture in pyrotechnics. The chemical components of this mixture are:[120] KNO_3—37%, $Na_2C_2O_4$—30%, Mg—30%, tars—3%. The specific energy of the mixture is 6 kJ/g and its luminous efficiency is 8 lm/W. The maximum combustion temperature is 2500–3000 K. The emission of the average ball lightning could account for 0.3 of that due to the firework material, and its chemical energy content is 3 g. By reducing the amount of sodium in the mixture by two orders of magnitude, we find that the luminous efficiency of the firework mateial becomes comparable with that of ball lightning.

The essential feature of the chemical process occurring in the firework material is that the oxidizing agent is drawn from the mixture itself (it is not atmospheric oxygen). This ensures that the reaction is fast, gives rise to a high temperature, and produces a source with high luminous efficiency. A similar conclusion about the combination of reacting components was previously made in respect of the chemical process in ball lightning. Apart from ozone, the oxides of nitrogen and sulfur, and the salts of nitric and sulfuric acids, can be oxygen-containing components of the atmosphere.

The last of the five aspects mentioned above refers to the electric properties of ball lightning. Observations[100] show that ball lightning is often attracted to metal objects, interacts with electrical systems, and sometimes appears from electrical instruments. Frequently, the effect of ball lightning on humans is similar to that of an electrical discharge. The question arises as to what is the source of the electric charge of ball lightning, which gives rise to its surface tension and stability, and what are the associated electrical phenomena?

The formation of electric charge occurs in parallel with the formation of the fractal cluster by the aggregation of solid particles. These particles are charged and, in the case of a spherical particle of radius r_0, the electric charge Z of a particle, expressed in units of the electron charge e, is[57]

$$Z=\frac{Tr_0}{e^2}\ln\frac{K_-}{K_+}, \tag{6.8}$$

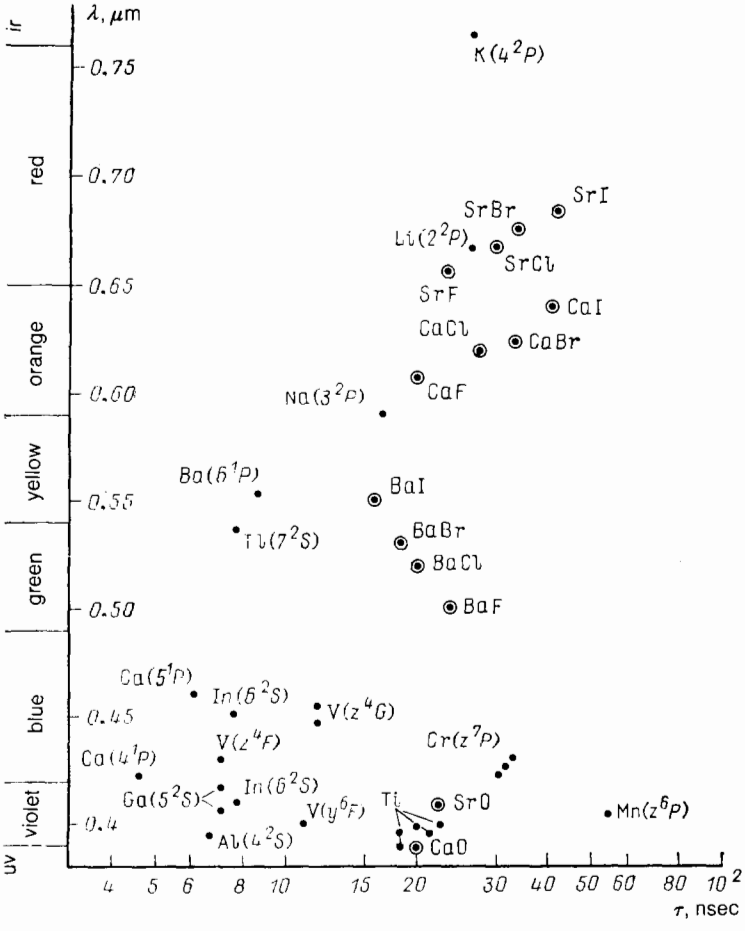

FIG. 15. Wavelengths corresponding to transitions to the ground state from the short-lived excited states of atoms and molecules radiating in the optical part of the spectrum. For molecules, we show the position of the transition between the main vibrational levels of the electronic transitions.

where K_-, K_+ are the mobilities of negative and positive ions in air. The type of ion in air and, consequently, its mobility, depend on humidity of and the impurities present in the atmosphere. If we average over the mobilities of ions in the air,[118,119] we obtain

$$\frac{Z}{r_0} = -6 \pm 2\ \mu n^{-1}.$$

The aggregation of negatively charged particles results in a negatively charged cluster. The significant point is that the flow of charge to the periphery of the cluster must occur more slowly than the formation of the cluster itself. The surface charge will not then impede the formation of a charged cluster.

To obtain some idea about the quantitative aspects of the process, let us consider the special case where a spherical fractal cluster of radius $R_0 = 10$ cm is assembled from particles of radius 1 μm, and its surface tension is equal to that of water (0.073 J/m^2). The surface tension α, determined by the electric charge q of the cluster, is

$$\alpha = \frac{q^2}{4\pi R_0^2} = \frac{E^2}{4\pi R_0}, \tag{6.9}$$

where E is the electric field near its surface. In the present case, $q = 1000$ cgs, $E = 300$ kV/m, and the cluster potential is 30 kV. If we use (5.1), we can show that the fractal dimension of the cluster is then $D = 2.31$, which is quite realistic (see Table III). As it flows toward the periphery of the cluster, the charge eventually concentrates at the ends, whose linear dimensions are of the order of 50 μm. An electric field of 30 mV/m is produced near the surface, and this is not high enough to generate a coronal discharge. The fractal cluster discharges under the influence of ions in the atmosphere and, when the ion density in the atmosphere is 100–1000 cm^{-3}, this occurs in a time of the order of 10 min, the ions being collected from a large volume of the atmosphere of the order of 1000–10 000 cm^3. Moreover, near the ends of the cluster, where the field strength exceeds 3 mV/m, the negative space charge in air is due to electrons. Collisions between the electrons and air molecules produce excitation of the latter and the associated emission. However, the emission is of low intensity (it is comparable with the intensity emitted by nocturnal insects).

Finally, we consider one further point associated with a property of the fractal cluster containing the active material of ball lightning. We note that, if this cluster is formed by the successive attachment of individual particles to it, its fractal dimension is 2.46 ± 0.05 (see Table III), and the cluster is optically opaque. If, on the other hand, it is formed by cluster-cluster aggregation, the fractal dimension of the cluster is 1.77 ± 0.03, and it is optically transparent. The choice between these two variants can be made if we know the optical thickness of ball lightning. It has frequently been reported that the observed ball lightning is optically transparent, but such reports can hardly be regarded as reliable. More specific information can be obtained by examining a photograph of ball lightning with a photometer. This was done in Ref. 53, in which a photograph of a ball lightning track made by V. M. Deryugin during a storm at the Karabad meteorological station in the Gur'evskiĭ region on 9 June 1958 at 21.30 hours.

Photometry of the ball lightning track can be used to determine how the amount of light reaching the film decreases in the lateral direction from the center of the track. Let us examine this in two limiting cases. The amount of light reaching the photograph is, of course, the integral of the instantaneous power with respect to time. We shall assume that the ball lightning is spherical, with radius R_0, and that it travels uniformly. Let us suppose that a given point receives radiation corresponding to impact parameter ρ, i.e., the minimum projected distance to the set of points in the ball lightning. If the ball lightning is optically opaque, the radiant power reaching a given point is the same throughout the exposure. Blackening is then proportional to the exposure time $2(R_0^2 - \rho^2)^{1/2}/v$, where v is the velocity of the ball lightning. This means that the relative blackening of the film is $[1 - (\rho^2/R_0^2)]^{1/2}$, where the blackening at the center of the track is taken to be equal to unity. A similar method can be used for optically transparent ball lightning to show that the relative blackening of the track is $1 - (\rho^2/R_0^2)$.

Figure 16 shows the results obtained by a photometric scan of the track of ball lightning,[53] using one of the above variants. If the ball lightning is optically transparent or optically opaque, the points on the corresponding graph should lie on the straight line $y = 1$. However, the points shown in Fig. 16 do not enable us to choose between the two limiting cases "by inspection," as was done in Ref. 53. Statistical analysis of the data in Fig. 16 shows that the average relative blackening obtained on the assumption that the ball lightning is optically opaque is $y = 0.81 \pm 0.16$, whereas the assumption of optical transparency gives $y = 0.96 \pm 0.17$. Although the transparent ball lightning should be given preference, these results are subject to considerable uncer-

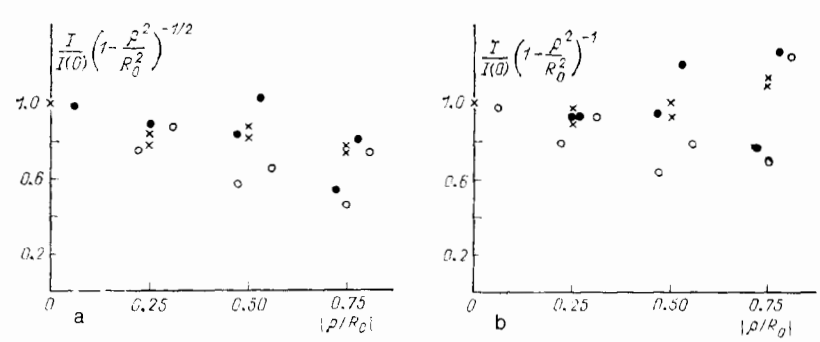

FIG. 16. Lateral photometric scan of the track of ball lightning. Relative blackening of the film in the direction at right-angles to the track, expressed in convenient units for two models: a—surface emission, b—volume emission. If the corresponding model is valid, and the ball lightning is spherical in shape and homogeneous, the points should lie on the $y = 1$ line.

tainty and a choice cannot be made. This analysis has shown that lateral photometric scans of the ball lightning track will yield useful information on the state of the active material in ball lightning, provided statistically significant material is available.

To conclude this section, we note that an understanding of the fact that the active material of ball lightning has the structure of a fractal cluster enables us to answer basic questions about ball lightning, and to provide a schematic picture of the phenomenon. Nevertheless, to develop laboratory models of ball lightning, it will be necessary to perform a more detailed examination of each of the above questions, using specific systems and conditions.

7. CONCLUSION

Fractal clusters are an intermediate stage in the formation of a condensed phase from solid aerosols. Information deduced about these structures will enable us in the near future to provide a detailed physical picture of the formation of the condensed phase and to elucidate the role of fractal clusters in the formation of condensed matter in gases and liquids.

Fractal clusters constitute one of the representations of systems with fractal structure. Since these are geometric systems, their analysis is simpler than many of the analogs of fractal clusters. Hence, information on fractal clusters will help us to understand the physical picture of different fractal-type structures and phenomena.

Studies of fractal clusters are also interesting from the purely methodological point of view. Experience gained as a result of such studies has shown that, at present, computer experiments constitute a very effective way of studying physical objects and phenomena, and their possibilities in this area are far more extensive than those of other methods.

We note in conclusion that the fractal cluster has entered modern physics as an interesting and widespread physical structure, and will continue to occupy a prominent place in physics.

[1)]We note that the word *cluster* is commonly taken to refer to a large number of bound atoms or molecules which retain their individuality within this system. This terminology was subsequently extended to systems consisting of a large number of bound macroscopic particles.

[2)]It is common to use the gyration radius to characterize the size of a cluster. It is given by $R_g = (\overline{R^2})^{1/2}$, where R is the distance of a cluster particle from its center of mass, and the bar represents averaging over the particle distribution in the cluster.

[3)]This model of forming a fractal cluster[6,7] is referred to as the cl-cl model (clustering of clusters) while the Witten-Sander model and its modifications are frequently referred to as DLA (diffusion-limited aggregation).

[4)]The same result follows from an analysis of computer simulations[55] in the case of a fractal cluster formed as a result of cluster-cluster aggregation.

[5)]The initial anisotropy of the system is of fundamental significance for the formation of fractal structures.[56,72,73]

[6)]The time t that has elapsed since the beginning of the motion and the number n of steps covered by the particle during this time are proportional to one another. Accordingly, (3.18) can be rewritten, for example, in the form $t \sim R^{D_\omega}$.

[7)]We note that, for the above distribution, the quantity F that appears in (4.7) is given by

$$F = \frac{1}{2} + \frac{1}{2}\langle r\rangle \left\langle \frac{1}{r} \right\rangle = 1.105,$$

where the angle brackets represent averaging over the aerosol distribution. This gives $k = 2.95T/\eta$ for the aerosol aggregation rate constant (4.7). This quantity is independent of not only the size of the aggregating aerosols, but also of their nature. In air at room temperature, the aggregation rate constant is 6.6×10^{-10} cm^3/s. The measured result[59] in units of 10^{-10} cm^3/s is 6.0 for ammonium chloride, 6.6 for iron oxide, 8.3 for magnesium oxide, 8.0 for cadmium oxide, 5.1 for stearic acid, 5.1 for oleic acid, 4.9 for tar, 5.0 for paraffin oil, and 6.3 for n-xylolazo-β-naphthanol. The statistical average of the experimental results is $(6\mp1)\times10^{-10}$ cm^3/s, which is in agreement with the above theoretical value and confirms that the dependence on the aerosol material is slight.

[8)]According to (4.13) and (4.14), when $\gamma = 0$, we have $a = D - 2\omega = D - (d - D_\omega)$. For Brownian particle motion ($D_\omega = 2$), this is identical with the above result.

[9)]We note, for comparison, that the particle diameter is greater by a factor of about 60 than the diameter of gold atoms, so that an individual particle contains roughly 10^5 gold atoms.

[10)]A different mixture is used for illumination purposes, namely, the oxidizing agent and the fuel are in the form of small particles that can be diluted by neutral components to slow down the chemical reaction.

[11)]The luminous efficiency of a source of light is equal to the ratio of the luminous flux produced by it to the power expended in producing it.[116]

[1]T. A. Witten and L. M. Sander, Phys. Rev. Lett. **47**, 1400 (1981).
[2]B. B. Mandelbrot, *The Fractal Geometry of Nature*, Freeman, San Franciso, 1982.
[3]G. I. Barenblatt, Podobie, avtomodel'nost', promezhutochnaya asimptotika, Gidrometeoizdat, Moscow, 1978 [Engl. transl., Similarity, Self-Similarity, and Intermediate Asymptotics, Plenum, 1980].
[4]Ya. B. Zel'dovich and D. D. Sokolov, Usp. Fiz. Nauk **146**, 493 (1985) [Sov. Phys. Usp. **28**, 608 (1985)].
[5]P. Meakin, Phys. Rev. A **27**, 604 (1983).
[6]P. Meakin, Phys. Rev. Lett. **51**, 1119 (1983).
[7]M. Kolb, R. Botet, and R. Jullien, *ibid.* 1123.
[8]P. Meakin, J. Colloid. Interface Sci. **102**, 491 (1985).
[9]R. Botet, R. Jullien, and M. Kolb, J. Phys. A **17**, L75 (1984).
[10]M. Plischke and Z. Racz, Phys. Rev. Lett. **53**, 415 (1984).
[11]Z. Racz and M. Plischke, Phys. Rev. A **31**, 985 (1985).
[12]P. Meakin, *ibid.* **27**, 1495 (1983).
[13]P. Meakin, J. Chem. Phys. **79**, 2426 (1983).
[14]M. Sahimi *et al.*, Phys. Rev. A **32**, 590 (1985).
[15]P. Meakin, *ibid.* **29**, 997 (1984).
[16]P. Meakin, J. Colloid Interface Sci. **96**, 415 (1983).
[17]M. Kolb, Phys. Rev. Lett. **53**, 1653 (1984).
[18]P. Meakin and Z. P. Wasserman, Phys. Lett. A **103**, 337 (1984).
[19]P. Meakin, Phys. Rev. B **29**, 2930 (1984).
[20]R. Jullien, M. Kolb, and R. Botet, J. Phys. (Paris) **45**, L211 (1984).
[21]R. Botet, R. Jullien, and M. Kolb, Phys. Rev. B **30**, 2150 (1984).
[22]R. Richter *et al.*, Bull. Am. Phys. Soc. **28**, 261 (1983).
[23]L. M. Sander, Z. M. Cheng, and R. Richter, Phys. Rev. B **28**, 6394 (1983).
[24]P. Garik, *ibid.* A **32**, 1275 (1985).
[25]F. W. Wiegel and A. S. Perelson, J. Stat. Phys. **29**, 813 (1982).
[26]Y. Sawada *et al.*, Phys. Rev. A **26**, 3557 (1982).
[27]Pattern Formation of Dynamic Systems and Pattern Recognition, ed. by H. Haken, Springer-Verlag, Berlin-Heidelberg-New York, 1979.
[28]H. G. E. Hentschel and I. Procaccia, Phys. Rev. Lett. **49**, 1158 (1982).
[29]H. G. E. Hentschel and I. Procaccia, Phys. Rev. A **27**, 1266 (1983).
[30]P. Meakin and L. M. Sander, Phys. Rev. Lett. **54**, 2053 (1984).
[31]T. A. Witten and L. M. Sander, Phys. Rev. A **27**, 5686 (1983).
[32]R. C. Ball *et al.*, Phys. Rev. Lett. **55**, 1406 (1985).
[33]P. Meakin, Phys. Rev. B **29**, 3722 (1984).
[34]P. Meakin, *ibid.* A **27**, 2616 (1983).
[35]H. G. E. Hentschel, Phys. Rev. Lett. **52**, 212 (1984).
[36]M. Muthukamar, *ibid.* **50**, 686 (1983).
[37]Z. Racz, Phys. Rev. A **32**, 1129 (1985).
[38]A. Z. Patashinskiĭ and V. L. Pokrovskiĭ, Fluktuatsionnaya teoriya fazovykh perekhodov (Fluctuation Theory of Phase Transitions), Nauka, Moscow, 1982 [English translation of 1975 edition, Pergamon, Oxford, 1979].
[39]P. Pfeuty and G. Toulouse, *Introduction to the Renormalization Group and to Critical Phenomena*, Wiley, New York, 1977.
[40]D. J. Amit, *Field Theory, the Renormalization Group and Critical Phenomena*, McGraw-Hill, New York, 1978.

[41]K. G. Wilson, Rev. Mod. Phys. **55**, 583 (1983) [Russ. transl. Usp. Fiz. Nauk **141**, 193 (1983)].
[42]H. Gould, F. Family, and H. E. Stanley, Phys. Rev. Lett. **50**, 686 (1983).
[43]S. Alexander and R. Orbach, J. Phys. (Paris) **43**, L625 (1982).
[44]R. Rammal and G. Toulouse, *ibid.* **44**, L13 (1983).
[45]S. Halvin and R. Nossal, Phys. A **17**, L427 (1984).
[46]M. Sahimi, *ibid.* 2567.
[47]P. Maekin and H. E. Stanley, Phys. Rev. Lett. **51**, 1457 (1983).
[48]Z. Djordjevic *et al.*, Phys. Rev. B **30**, 478 (1984).
[49]J. Vannimenus, J. P. Nadal, and J. Martin, J. Phys. A. **17**, L351 (1984).
[50]R. Botet, R. Jullien, and N. Kolb, Phys. Rev. A **30**, 2150 (1984).
[51]M. Kolb and R. Jullien, J. Phys. (Paris) **45**, L977 (1984).
[52]P. Meakin, J. Chem. Phys. **81**, 4637 (1984).
[53]M. T. Dmitriev, V. M. Deryugin, and G. A. Kalinkevich, Zh. Tekh. Fiz. **42**, 2187 (1972) [Sov. Phys. Tech. Phys. **17**, 1724 (1972)].
[54]P. Meakin, J. Chem. Phys. **83**, 3645 (1985).
[55]P. Meakin, J. Colloid. Interface Sci. **102**, 491 (1984).
[56]R. C. Ball *et al.*, Phys. Rev. Lett. **55**, 1406 (1985).
[57]N. A. Fuks, Mekhanika aerozolei (Mechanics of Aerosols), Academy of Sciences of the USSR, Moscow, 1955.
[58]M. V. Smoluchowski, Z. Phys. **17**, 585 (1916).
[59]H. L. Green and W. R. Lane, *Particulate Clouds: Dusts, Smokes, and Mists*, Spon, 1957 [Russian translation, Khimiya, Leningrad, 1972, p. 147].
[60]Kinetics of Aggregation and Gelation, ed. by F. Family and D. P. Landau, North-Holland, Amsterdam, 1984.
[61]R. Botet and R. Jullien, J. Phys. A **17**, 2517 (1984).
[62]T. Vicsek and F. Family, Phys. Rev. Lett. **52**, 1669 (1984).
[63]P. Meakin, T. Vicsek, and F. Family, Phys. Rev. B **31**, 564 (1985).
[64]J. M. Deutsch and P. Meakin, J. Chem. Phys. **77**, 2093 (1983).
[65]M. Nauenberg, Phys. Rev. B **28**, 449 (1983).
[66]H. J. Herrmann, D. P. Landau, and D. Stauffer, Phys. Rev. Lett. **49**, 412 (1982).
[67]H. J. Herrman, D. Stauffer, and D. P. Landau, J. Phys. A **16**, 1221 (1983).
[68]K. Friedlander, *Smoke, Dust, Haze: Fundamentals of Aerosol Behavior*, Wiley, New York, 1977.
[69]D. Beischer, Z. Electrochem. **44**, 375 (1938).
[70]T. Vicsek, P. Meakin, and F. Family, Phys. Rev. A **32**, 1122 (1985).
[71]P. Meakin and J. M. Deutsch, J. Chem. Phys. **83**, 4086 (1985).
[72]L. M. Sander, P. Ramandal, and E. Ben-Jacob, Phys. Rev. **32**, 3156 (1985).
[73]E. Ben-Jacob *et al.*, Phys. Rev. Lett. **55**, 1315 (1985).
[74]S. R. Forrest and T. A. Witten, J. Phys. A **12**, L109 (1979).
[75]D. Weitz and M. Oliveria, Phys. Rev. Lett. **52**, 1433 (1984).
[76]W. T. Elam *et al.*, *ibid.* 54, 701 (1985).
[77]M. Matsushita *et al.*, *ibid.* **53**, 286 (1984).
[78]D. W. Schaefer and K. D. Keefer, *ibid.* 1383.
[79]D. W. Schaefer *et al.*, *ibid.* **52**, 2371.
[80]V. Ya. Aleksandrov, I. P. Borodin, E. V. Kichenko, and I. V. Podmoshenskiĭ, Zh. Tekh. Fiz. **52**, 818 (1982) [Sov. Phys. Tech. Phys. **27**, 527 (1982)].
[81]L. Niemeyer, L. Pietronero, and H. J. Weismann, Phys. Rev. Lett. **52**, 1033 (1984).
[82]J. Nittmann, G. Daccord, and N. E. Stanley, Nature **314**, 141 (1985).
[83]P. Pfeifer and D. Avnir, J. Chem. Phys. **79**, 3558 (1983).
[84]D. Avnir, D. Farin, and P. Pfeifer, J. Chem. Phys. **79**, 3566 (1983).
[85]H. D. Bale and P. W. Schmidt, Phys. Rev. Lett. **53**, 596 (1984).
[86]D. Avnir, D. Farin, and P. Pfeifer, Nature **308**, 261 (1984).
[87]A. J. Katz and A. H. Thompson, Phys. Rev. Lett. **54**, 1325 (1985).
[88]C. Amitranov, A. Bunde, and H. E. Stanley, J. Phys. A **18**, L923 (1985).
[89]V. Ya. Aleksandrov, E. M. Golubev, and I. V. Podmoshenskiĭ, Zh. Tekh. Fiz. **52**, 1987 (1982) [Sov. Phys. Tech. Phys. **27**, 1221 (1982)].
[90]F. Arago, Thunder and Lightning [translated from French, St. Petersburg, 1859].
[91]W. Brand, Der Kügelblitz, H. Grand. Hamburg, 1923.
[92]W. J. Humphreys, Sci. News Lett. **20**, 73 (1931).
[93]W. J. Humphreys, Proc. Am. Philos. Soc. **76**, 613 (1936).
[94]R. Leonov, Zagadka sharovoĭ molnii (The Puzzle of Ball Lightning), Nauka, Moscow, 1965.
[95]J. R. McNally, "Preliminary report on the ball lightning," ORNL-3938, Oak Ridge Nat. Lab., May, 1966.
[96]W. D. Rayle, "Ball lightning characteristics," NASA Techn. Note, NASA-TN-D-3188, 1966.
[97]M. T. Dmitriev, Priroda No. 6, 50 (1971).
[98]S. Singer, Nature of Ball Lightning, Plenum, 1971 [Russian translation, Mir, Moscow, 1973].
[99]W. N. Charman, Phys. Rep. **54**, 261 (1979).
[100]I. P. Stakhanov, Fizicheskaya priroda sharovoĭ molnii (Physical Nature of Ball Lightning), Atomizdat, Moscow, 1979.
[101]I. Imyanitov and D. Ya. Tikhiĭ, Za gran'yu zakona (Beyond the Law), Atomizdat, Moscow, 1980.
[102]J. D. Barry, *Ball Lightning and Bead Lightning*, Plenum, 1980 [Russian translation, Mir, Moscow, 1983].
[103]B. M. Smirnov, Problema sharovoĭ molnii (The Problem of Ball Lightning), Nauka, Moscow.
[104]B. M. Smirnov, Usp. Fiz. Nauk **116**, 731 (1975) [Sov. Phys. Usp. **18**, 636 (1975)].
[105]B. M. Smirnov, Dokl. Akad. Nauk SSSR **226**, 806 (1976) [Sov. Phys. Dokl. **21**, 89 (1976)].
[106]B. M. Smirnov, Zh. Tekh. Fiz. **47**, 830 (1977) [Sov. Phys. Tech. Phys. **22**, 488 (1977)].
[107]B. M. Smirnov, Khimiya plazmy (Plasma Chemistry), Atomizdat, Moscow, 1976, No. 4, p. 191.
[108]A. O. Nazaryan, V. G. Plyukhin, and B. M. Smirnov, "Thermal processes accompanying the interaction between ozone and charcoal," Preprint ITF SO AN SSSR No. 121, Novosibirsk, 1985.
[109]A. O. Nazaryan, V. G. Plyukhin, and B. M. Smirnov, Khimiya plazmy (Plasma Chemistry), Energoatomizdat, Moscow, 1986, No. 14.
[110]V. G. Plyukhin and B. M. Smirnov, Dokl. Akad. Nauk SSSR (1986) [*sic*].
[111]V. P. Kraĭnov, B. M. Smirnov, and I. P. Shmatov, *ibid.* **283**, 361 (1985) [Sov. Phys. Dokl. **30**, 587 (1985)].
[112]Ya. B. Zel'dovich, Zh. Eksp. Teor. Fiz. **7**, 1463 (1937); Izbrannye Tr. I., Nauka, Moscow, 1984, p. 74.
[113]L. D. Landau and E. M. Lifshitz, Mekhanika sploshnykh sred, Gostekhizdat, 1953, §56, Problem 4, p. 267 [English translation, Fluid Mechanics, Pergamon Press, Oxford, 1959].
[114]V. P. Kraĭnov, G. P. Lebedev, A. O. Nazaryan, and B. M. Smirnov, Zh. Tekh. Fiz. (1986) [*sic*].
[115]L. D. Landau and E. M. Lifshitz, Elektrodinamika sploshnykh sred (Electrodynamics of Continuous Media), Nauka, Moscow, 1982, p. 420 [English translation, Pergamon Press, Oxford, 1984].
[116]L. A. Sena, Edinitsy fizicheskikh velichin (Units of Physical Quantities), Nauka, Moscow, 1973.
[117]E. A. Andreev and E. E. Nikitin, see Ref. 107, p. 28.
[118]N. V. Krasnogorskaya, Elektrichestvo nizhnikh sloev atmosfery i metody ego izmereniya (Electricity in the Lower Layers of the Atmosphere and Methods for Its Measurement), Gidrometeoizdat, Leningrad, 1972.
[119]A. Hussin *et al.*, J. Aerosol Sci. **14**, 671 (1983).
[120]A. A. Shidlovskiĭ, Osnovy pirotekhniki (Fundamentals of Pyrotechnics), Mashinostroenie, Moscow, 1973.

Translated by S. Chomet